NASA TECHNICAL NOTE

NASA TN D-6692

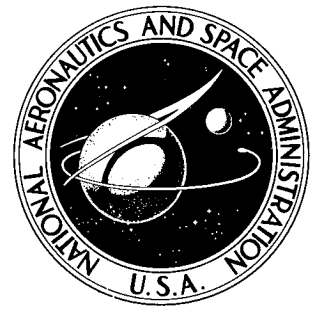

NASA TN D-6692

STRUCTURAL WEIGHT ANALYSIS OF HYPERSONIC AIRCRAFT

by Mark D. Ardema

Office of Advanced Research and Technology
Advanced Concepts and Missions Division
Moffett Field, Calif. 94035

NATIONAL AERONAUTICS AND SPACE ADMINISTRATION • WASHINGTON, D. C. • MARCH 1972

1. Report No.	2. Government Accession No.	3. Recipient's Catalog No.
NASA TN D-6692		

4. Title and Subtitle	5. Report Date
STRUCTURAL WEIGHT ANALYSIS OF HYPERSONIC AIRCRAFT	March 1972
	6. Performing Organization Code

7. Author(s)	8. Performing Organization Report No.
Mark D. Ardema	A–3905
	10. Work Unit No.
	130–06–17–11–15

9. Performing Organization Name and Address	11. Contract or Grant No.
Office of Advanced Research and Technology Advanced Concepts and Missions Division Moffett Field, California 94035	
	13. Type of Report and Period Covered
	Technical Note

12. Sponsoring Agency Name and Address	14. Sponsoring Agency Code
National Aeronautics and Space Administration Washington, D.C. 20546	

15. Supplementary Notes

16. Abstract

The weights of major structural components of hypersonic, liquid hydrogen (LH_2) fueled aircraft are estimated and discussed. The major components are the body structure, body thermal protection system, tankage, and wing structure. The method of estimating body structure weight is presented in detail in this paper, while the weights of the other components are estimated by methods given in referenced papers. Two nominal vehicle concepts are considered: the advanced concept employs a wing-body configuration and hot structure with a nonintegral tank, while the potential concept employs an all body configuration and cold, integral "pillow" tankage structure. Characteristics of these two concepts are discussed and parametric data relating their weight fractions to variations in vehicle shape and size, design criteria and mission requirements, and structural arrangement are presented. Although the potential concept is shown to have a weight advantage over the advanced, it involves more design uncertainties since it is farther removed in design from existing aircraft.

17. Key Words (Suggested by Author(s))	18. Distribution Statement
Structural analysis Weight estimation Hypersonic aircraft	Unclassified – Unlimited

19. Security Classif. (of this report)	20. Security Classif. (of this page)	21. No. of Pages	22. Price*
Unclassified	Unclassified	52	$3.00

*For sale by the National Technical Information Service, Springfield, Virginia 22151

TABLE OF CONTENTS

SYMBOLS

A	cross sectional area, m^2 (ft^2)
A_B	body surface area, m^2 (ft^2)
A_F	frame cross-sectional area, cm^2 ($in.^2$)
a	semimajor axis, m (ft)
a_M	maximum semimajor axis, m (ft)
b	semiminor axis, m (ft)
b_M	maximum semiminor axis, m (ft)
C_F	Shanley's constant
C_{MW}	wing materials coefficient
D	maximum diameter of wing-body, m (ft)
d	frame spacing, cm (in.)
d_F	frame cross-section semidepth, cm (in.)
d_i	defined on figure 26, m (ft)
d_T	body depth at vertical tail, m (ft)
E	Young's modulus, N/m^2 ($lb/in.^2$)
E_I	complete elliptic integral of first kind
E_{II}	complete elliptic integral of second kind
E_{III}	defined by equation (C4)
e	eccentricity, defined by equation (A19)
F_{cy}	compressive yield strength, N/m^2 ($lb/in.^2$)
F_{tu}	tensile ultimate strength, N/m^2 ($lb/in.^2$)
I_F	frame cross-section moment of inertia, cm^4 ($in.^4$)
I_y	moment of inertia about y axis, cm^4 ($in.^4$)

I'_y	$I_y/\bar{t}_s$, cm^3 ($in.^3$)
K_{F1}	defined by equation (B8)
K_{F2}	defined by equation (B9)
K_{mg}	shell minimum gage factor, see equation (B6)
K_p	shell geometry factor for hoop stress
K_S	frame spring constant, N/m (lb/in.)
K_{TPS}	TPS nonoptimum factor
L_T	maximum vertical tail lift, N (lb)
ℓ	body length, m (ft)
ℓ_π	distance to breakpoint, see figure 24, m (ft)
M	longitudinal bending moment, N-m (lb-ft)
M_C	cruise Mach number
m	buckling equation exponent
N_S	stress resultant in shell, N/m (lb/in.)
N_W	stress resultant in wall, N/m (lb/in.)
N_x^+	tensile axial stress resultant, N/m (lb/ft)
N_x^-	compressive axial stress resultant, N/m (lb/ft)
N_y	hoop direction stress resultant, N/m (lb/ft)
n	load factor
P	perimeter, m (ft)
P_g	shell internal gage (differential) pressure, N/m^2 ($lb/in.^2$)
P_s	perimeter of shell, m (ft)
P_w	perimeter of walls, m (ft)
p	exponent of power law of wing-body, see figure 24

R_{BR} breakpoint ratio, defined by equation (A9)

R_{fat} fatness ratio, defined by equation (A8)

R_{fin} fineness ratio, defined by equation (A3)

r radius of wing-body, m (ft)

r_i defined on figure 26, m (ft)

S_p plan area of lifting surface, m^2 (ft^2)

S_π breakpoint cross-sectional area of all-body, m^2 (ft^2)

T temperature, °K (°F)

$\bar{T}$ mean temperature, °K (°F)

t time, ks (hours)

t_g material gage thickness, $\bar{t}_S/K_{mg}$, cm (in.)

t_{mg} material minimum gage thickness, cm (in.)

$\bar{t}$ total equivalent isotropic thickness of shell and frames, cm (in.)

$\bar{t}_F$ smeared equivalent isotropic thickness of frames, cm (in.)

$\bar{t}_{F_B}$ smeared frame thickness required to prevent failure caused by buckling, cm (in.)

$\bar{t}_{F_P}$ smeared frame thickness required to prevent failure caused by pressure bending, cm (in.)

$\bar{t}_S$ equivalent isotropic thickness of shell, cm (in.)

$\bar{t}_{S_B}$ shell thickness required to preclude buckling failure, cm (in.)

$\bar{t}_{S_C}$ shell thickness required to preclude compressive failure, cm (in.)

$\bar{t}_{S_G}$ shell thickness required to meet minimum gage constraint, cm (in.)

$\bar{t}_{S_T}$ shell thickness required to preclude tensile failure, cm (in.)

$\bar{t}_T$ smeared tension tie thickness, cm (in.)

$\bar{t}_w$ smeared wall thickness, cm (in.)

$\bar{t}_{w_G}$ thickness of wall to meet minimum gage constraint, cm (in.)

$\bar{t}_{w_T}$	thickness of wall required to prevent tensile failure, cm (in.)
U_{const}	constant unit weight of TPS, N/m^2 ($lb/in.^2$)
U_{CP}	unit weight of cover panels, N/m^2 ($lb/in.^2$)
U_{ins}	unit weight of insulation plus boiloff, N/m^2 ($lb/in.^2$)
V_B	body volume, m^3 (ft^3)
(W/S)	wing loading, N/m^2 (lb/ft^2)
W_{BS}	weight of body structure, N (lb)
W_I	ideal body weight, see equations (B17) and (B34), N (lb)
W_{SB}	weight of spanwise beam, N (lb)
W_{TK}	weight of tank, N (lb)
W_{TO}	gross takeoff weight, N (lb)
W_{TPS}	weight of TPS, N (lb)
W_{wing}	wing weight, N (lb)
x	longitudinal body coordinate, m (ft)
y	transverse body coordinate, m (ft)
z	vertical body coordinate, m (ft)
β	body angle of all-body, rad
δ	frame deflection, cm (in.)
ϵ	shell buckling efficiency
η	volumetric efficiency of body structure
θ	intersection angle for pillow tanks, rad (deg)
θ_i	defined on figure 26, rad (deg)
Λ	sweep, rad (deg)
ρ	material density, kg/m^3 ($lb/in.^3$)

ρ_B	gross body density, kg/m^3 (lb/ft^3)
ϕ	payload performance, N (lb)

STRUCTURAL WEIGHT ANALYSIS OF HYPERSONIC AIRCRAFT

Mark D. Ardema

Office of Advanced Research and Technology
Advanced Concepts and Missions Division
Moffett Field, California 94035

SUMMARY

The weights of major structural components of hypersonic, liquid hydrogen (LH_2) fueled aircraft are estimated and discussed. The major components are the body structure, body thermal protection system, tankage, and wing structure. The method of estimating body structure weight is presented in detail in this paper, while the weights of the other components are estimated by methods given in referenced papers. Two nominal vehicle concepts are considered: the advanced concept employs a wing-body configuration and hot structure with a nonintegral tank, while the potential concept employs an all-body configuration and cold, integral "pillow" tankage structure. Characteristics of these two concepts are discussed and parametric data relating their weight fractions to variations in vehicle shape and size, design criteria and mission requirements, and structural arrangement are presented. Although the potential concept is shown to have a weight advantage over the advanced, it involves more design uncertainties since it is farther removed in design from existing aircraft.

INTRODUCTION

This paper presents the weight analysis of the body structure of liquid hydrogen fueled hypersonic aircraft and discusses the weight characteristics of selected hypersonic aircraft designs. The weight items considered in addition to the load-carrying body structure are the body fuel tank, the body thermal protection system, and the wing. Not all these items will be needed for every design. These four weight items constitute the major portion of the dry weight of hypersonic aircraft; for a typical cruise vehicle they account for about 35 percent of the gross takeoff weight (the total dry weight is about 55 percent of gross). The weight of the remaining items (propulsion system, landing gear, surface controls, fixed equipment) does not vary substantially with changes in vehicle concept. Thus, to a first approximation, the sensitivity of vehicle dry weight to design parameters may be assessed by considering the four weight items mentioned above.

Preliminary weight estimates of aircraft traditionally have been made using empirical methods based on the weights of existing aircraft. Reference 1 describes such methods, and references 2 and 3 apply them to hypersonic aircraft. Studies have shown, however, that the bodies or fuselage designs of hypersonic aircraft will be significantly different from those of existing aircraft (refs. 4–11). The most important of these differences are the requirement for containment of cryogenic fuel in the body, the presence of insulated structure, and possibly the employment of noncircular structural shells. These differences suggest the need for an analytically based method of arriving at preliminary body weight estimates rather than methods relying on historical data. On the

other hand, in a preliminary design effort such as that in progress for hypersonic aircraft, a large number of vehicle designs must be rapidly evaluated. This requirement precludes the use of detailed methods of structural analysis at present, and body structure weight for preliminary design purposes must be computed on the basis of idealized vehicle models and simplified structural analysis.

The development and application of an analytical method based on beam theory for estimating body weight is presented in detail in this paper. The analysis considers only yield strength and buckling failure modes; it cannot be employed in place of a detailed design study for making final design decisions or for determining accurate weights. The analysis has been programmed for a digital computer to yield rapid estimates. The program is well suited both for weight-sensitivity studies and for incorporation as a subprogram in a mission performance model.

One of the most important considerations in preliminary design is configuration selection. For hypersonic aircraft, there is a trend toward configurations in which the vehicle wing and body are somewhat blended. The limiting case of this trend is the all-body configuration, which has no structure designed solely to produce lift. From a weight standpoint, the all-body shape appears to have both inherent advantages and disadvantages when compared with the conventional wing-body shape. Among the advantages are the elimination of the wing and smaller overall dimensions. Principal disadvantages are greater body surface areas and noncircular structural sections. Both configurations are considered in this paper.

For hypersonic aircraft, basic questions arise concerning the arrangement of the body structure (ref. 12). For example, the structure may be either exposed to the atmosphere ("hot" structure) or protected from atmospheric heating by an insulation system ("cold" structure). The fuel tank may be either separate from the body structure (nonintegral tankage) or combined with the body structure as one unit (integral tankage). Wing-body versus all-body, hot structure versus cold structure, and nonintegral versus integral tankage are compared and discussed.

The primary purpose of this paper is to present and discuss parametric (weight sensitivity) data for hypersonic aircraft. Weight sensitivity data are presented for two nominal designs or concepts. The "advanced" concept employs a wing-body configuration, hot structure, and a nonintegral tank. The "potential" concept uses an all-body configuration and a cold, integral pillow tank structure consisting of intersecting conical shells. Characteristics of these nominal designs are discussed and results are presented relating variations in weight with parameters in the following areas: (1) vehicle size and shape, (2) design criteria and mission requirements, and (3) structural design.

METHOD OF ANALYSIS

The vehicle configurations considered in this study are shown in figure 1, and their geometrical relationships are presented in appendix A. The wing-body configuration consists of a double-ended, power-law body of circular cross section and a delta wing. The all-body arrangement is composed of an elliptical-cone forebody with an afterbody of elliptical cross section, which fairs to a straight-line trailing edge. These shapes were chosen both because they are easily described in mathematical form and because they represent well two designs currently of interest in hypersonic studies. The body structure is a shell in the same shape as the body configuration for all concepts

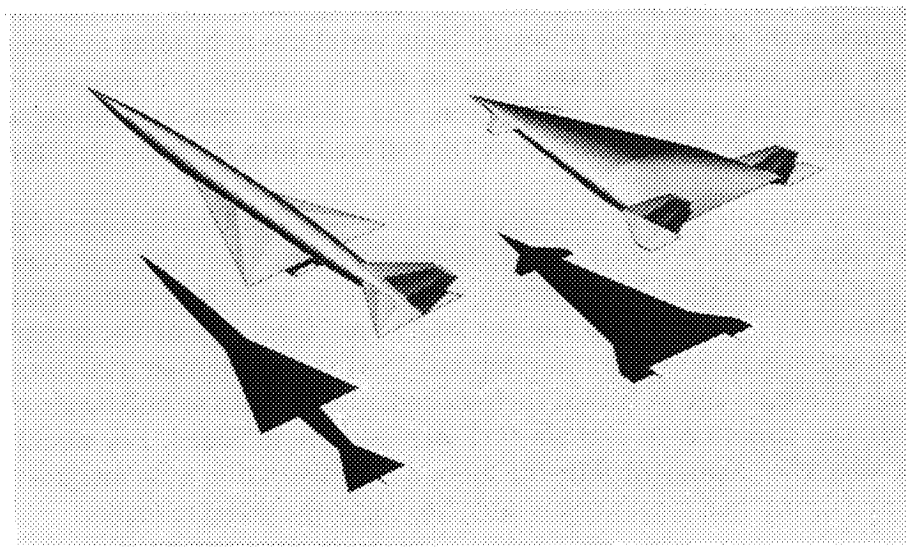

Figure 1.– Hypersonic aircraft configurations.

except those employing pillow tankage. In the pillow tankage concepts, intersecting conical tanks are fitted within the all-body configuration as described in appendix A and illustrated in figure 2.

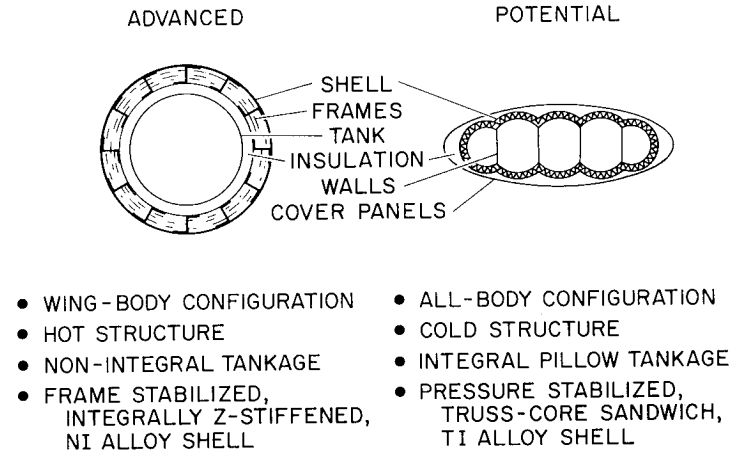

Figure 2.– Nominal structural concepts.

The loads were computed by methods described in reference 13. Briefly, longitudinal bending-moment distributions were based on vehicle loading due to a static maneuver (2.5 g pullup), a dynamic gust condition (15.25 m/s (50 fps) vertical wind shear), and a dynamic landing impact (3.05 m/s (10 fps) sink speed). A safety factor of 1.5 was applied to all loading conditions.

The resulting bending moments at each longitudinal body station were used to compute the amount of structural material required at the point of maximum stress. This material was distributed uniformly around the circumference, as is commonly done in preliminary weight analysis (cf. ref. 14, sec. 15.6). The portion of the material at the sides of the body not required for

resisting bending loads was assumed sufficient for resisting shear and torsion loads. Although variations in structural body weight arise primarily from variations in bending moment, loads due to pressurization were also accounted for and used to relieve compressive bending loads (pressure stabilization) in integral tank concepts. In addition, the all-body concepts incorporate sufficient spanwise structure in the aft sections to introduce the tail loads into the body structure.

Two structural arrangements are considered: an integrally Z-stiffened shell stabilized with ring frames, and a truss-core sandwich shell without frames. The structural materials considered are an aluminum alloy, a titanium alloy, a high-strength nickel alloy, and a high-temperature nickel alloy. The values of mechanical properties used for this study are 70 percent of the minimum values for procurement specification purposes given in reference 15 at the appropriate structural temperature. For integral tankage concepts the weight of such secondary structures as bulkheads and other items necessary to enable the structure to contain fuel must also be included. For nonintegral tanks, a separate fuel tank weight is computed. For the all-body configuration with integral tankage, either pillow tankage is used or internal truss-work is added to carry the pressure loads.

Appendix B gives in detail the body structural weight analysis, which assumes that the material exhibits elastoplastic behavior. Tensile yield, compression yield, and buckling failures are accounted for; in addition, there is a minimum gage restriction on the shell. The maximum stress failure theory was used for predicting yield failures. This theory results in very nearly the same weight estimates as can be obtained with failure theories based on biaxial states of stress. Buckling calculations assume the stiffened shell concepts to behave as wide columns and the sandwich shell concepts to behave as cylinders. The buckling equations, based on the results of reference 16, are derived in appendix C. The "nonoptimum" weights, which amount to about 40 percent of the body structure weight, are determined by an empirical method based on existing aircraft, as described in appendix B. The same nonoptimum factor is used for all concepts, even though sandwich structures might be expected to have higher nonoptimum weights because of the need for greater reinforcement in the vicinity of joints and cutouts. Since a circular section may be viewed as a special case of an elliptical section, the analyses of appendixes B and C are made for the all-body configuration and reduced to the wing-body as a special case.

The frames required for the stiffened shell concept are sized by the Shanley criterion (chap. 3, ref. 14). This criterion is based on the premise that, to a first-order approximation, the frames act as elastic supports for the wide column (p. 405, ref. 17; and p. 490, ref. 18), and it is widely used for weight estimation of ring-stiffened shell structures (refs. 19, 20, 21). Recent analyses based on more exact buckling models have indicated that in certain cases Shanley's criterion may either significantly overestimate or underestimate buckling loads for general stability (refs. 22, 23). For the structural arrangements considered in this paper (internally stiffened shells, $d/r \approx 0.2$) the Shanley criterion appears to be conservative. The criterion is extended to elliptical shells in appendix C, where it is shown that weight is relatively insensitive to the value of Shanley's constant.

Because nonoptimum weight is determined by comparison with existing subsonic aircraft, some phenomena peculiar to hypersonic vehicles are neglected in the analysis. Perhaps most important of these phenomena is the thermal environment. The high exterior temperature of the vehicle and the cryogenic temperature of the interior cause high thermal gradients, which may lead to significant thermal stresses, particularly in integral tankage concepts. However, a rough calculation based on the methods of reference 24 (chap. 10) indicates thermal stresses to be approximately an order of magnitude less than the bending stresses for the integral tankage

concepts considered here. Thus, although the thermal stresses may be high in certain local portions of the structure, the effect on the total weight may be expected to be small. This is in agreement with reference 7 which states that estimated thermal stresses cause about a 5 to 10 percent increase in weight. The thermal stresses in thin structures such as wings, on the other hand, may be expected to be significantly higher and, in fact, have been found to be approximately equal to bending stresses (ref. 25).

Another aspect of the thermal environment, the effects of high temperature on the physical properties of structural materials, can result in complex failure mechanisms involving fatigue, stress-corrosion, creep, and thermal cycling all of which are beyond the scope of this study. It is assumed that using 70 percent of long-time, at-temperature material properties will account for such phenomena to a major extent. Also neglected is the weight of such high temperature materials as refractory metals, which may be required in portions of the vehicle exposed to the highest temperatures, such as the nose and wing leading edges.

The methods used to estimate the weight of the tankage, the thermal protection system, and the wing are discussed briefly in appendix B. Tankage weight is estimated using information from reference 26 which describes the design, fabrication, and testing of a flight-weight liquid hydrogen tank and thermal protection system. Insulation thicknesses for thermal protection systems are computed from the transient heat conduction analysis described in reference 27; the calculation of the nonoptimum weight of this system utilizes information from reference 26. Although many thermal protection system concepts have been proposed (refs. 28 and 29) the only concept considered here is a passive system using helium-purged, quartz-fiber insulation. As noted earlier, wing weight is estimated by an empirical relationship from reference 3.

RESULTS

Characteristics of Nominal Concepts

The results of the weight study are presented primarily in the form of sensitivities of the weight of two nominal concepts to various parameters. The "advanced" concept represents the most conventional approach to hypersonic aircraft and would entail relatively little innovation and development. The "potential" concept represents a substantial departure from conventional aircraft designs and hence involves many more design uncertainties than the advanced concept. It must be remembered that to assess mission performance, aerodynamic and propulsion system characteristics must be considered as well as the dry weight fraction. The aerodynamic and propulsion system characteristics of the all-body configuration are analyzed in references 30 and 31, respectively, and the mission performance of this configuration is reported in references 10 and 11.

Figure 2 shows the structural arrangement of the advanced concept, which uses the wing body configuration shown in figure 3(a). The vehicle gross takeoff weight is 2220 KN (500,000 lb), the body volume is 2020 m^3 (71,400 ft^3), and the body length is 95 m (312 ft). The nominal mission is a 10.2 Mm (5500 n. mi.) cruise at a Mach number of 7. The hot, load-carrying, body structure of this design consists of an integrally Z-stiffened shell stabilized with ring frames. The structural

material is a nickel alloy, and the structure is designed for an internal pressure of 13,800 N/m^2 (2 psi) (not pressure stabilized). The fuel tank is nonintegral and has a helium-purged, quartz-fiber insulation system.

Figure 2 also shows the structural arrangement of the potential concept, which uses the all-body configuration shown in figure 3(b). The nominal vehicle size and mission are the same as for the advanced concept. The potential design has a cold, integral, pillow tank, load-carrying body structure consisting of a truss-core sandwich shell and monocoque walls, pressure stabilized at 69,000 N/m^2 (10 psi). The structural material is titanium alloy. Exterior nickel alloy cover panels and helium-purged quartz-fiber insulation are required for thermal protection of the pillow tankage structure.

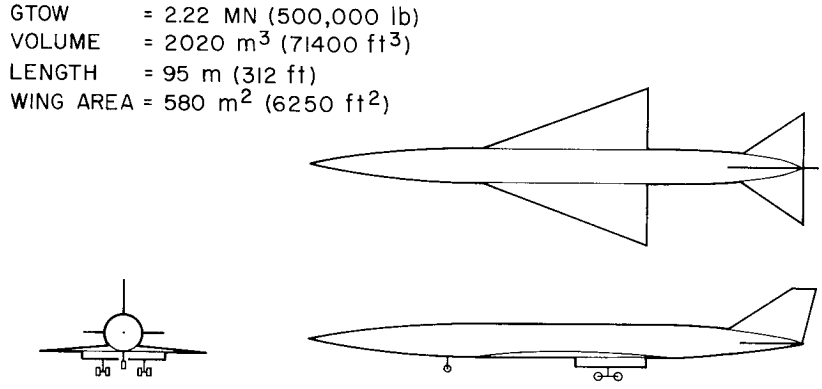

(a) Wing-body.

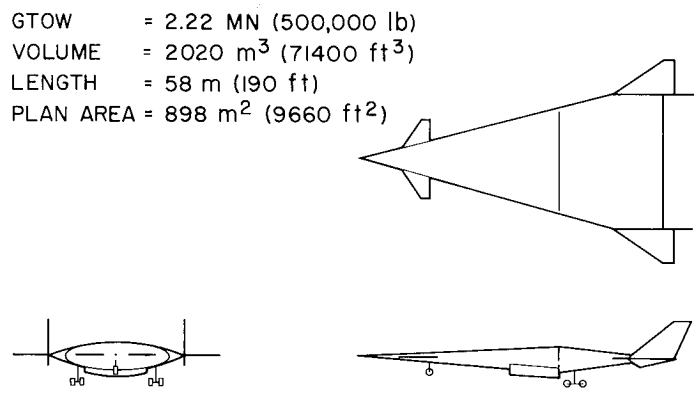

(b) All-body.

Figure 3.– Configurations.

Figure 4 shows the longitudinal bending moments as a function of body station for the two configurations; note that the magnitudes of the bending moments are approximately the same for both. The characteristics of the bending moment distributions are described in reference 13. For the

loading conditions chosen, both the all-body and the wing-body maneuver and landing conditions are dominant, while the gust condition does not significantly affect vehicle loadings. The three loads were assumed to act independently.

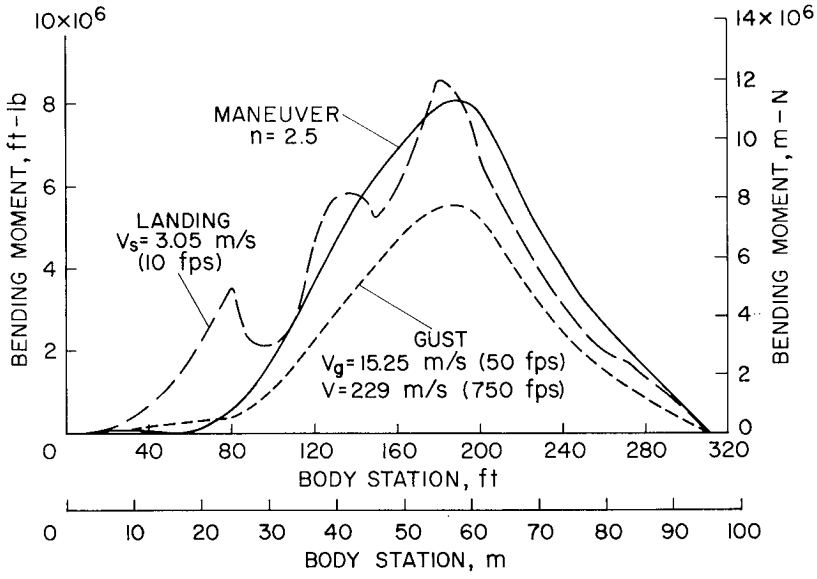

(a) Wing-body.

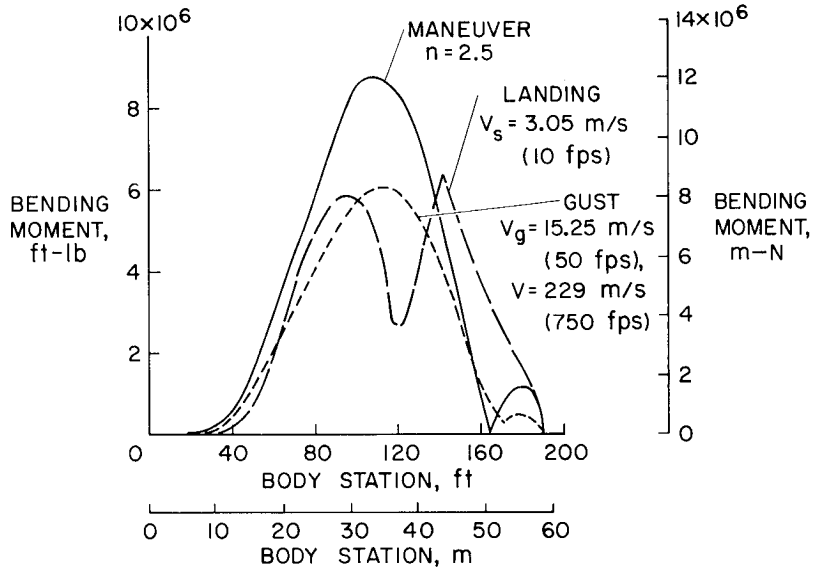

(b) All-body.

Figure 4.– Bending moments.

The unit weights of the shell and frames (weight per unit body wetted surface area) of the advanced concept, and of the shell and walls of the potential concept, are shown on figure 5. These curves have generally the same shape as the bending moment distributions of figure 4. For both concepts the structures are buckling limited, except for portions at the front and rear that are limited by a shell minimum gage constraint. The smallest allowable thickness of any structural elements was assumed to be 0.0254 cm (0.01 in.). The potential concept is more restricted by the minimum gage constraint than the advanced. The overall average unit masses (weights) of the load-carrying body structures (including nonoptimum mass and, in the case of the potential concept, bulkhead and spanwise beam mass) are 22 kg/m^2 (4.5 lb/ft^2) for the advanced concept and 13.2 kg/m^2 (2.7 lb/ft^2) for the potential.

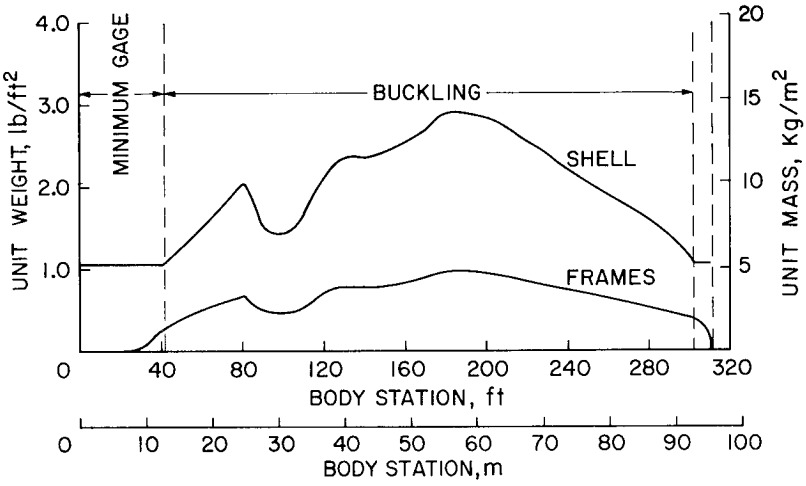

(a) Advanced.

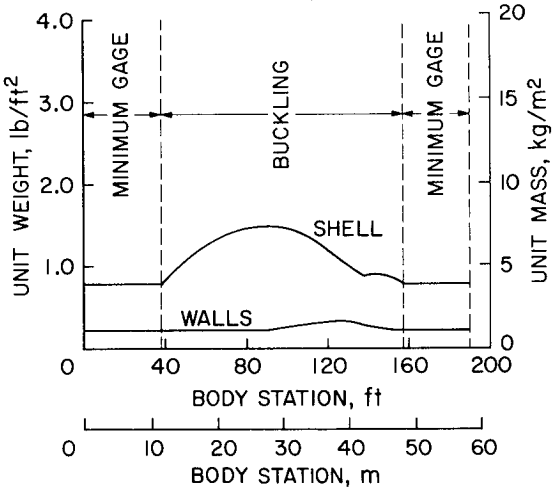

(b) Potential.

Figure 5.– Unit weights.

Figure 6 shows the equivalent isotropic thickness $\bar{t}$ – that is, the thickness of an equal mass isotropic shell – and gage thickness, t_g as a function of body station. These curves are, of course proportional to the unit weight curves of the previous figure.

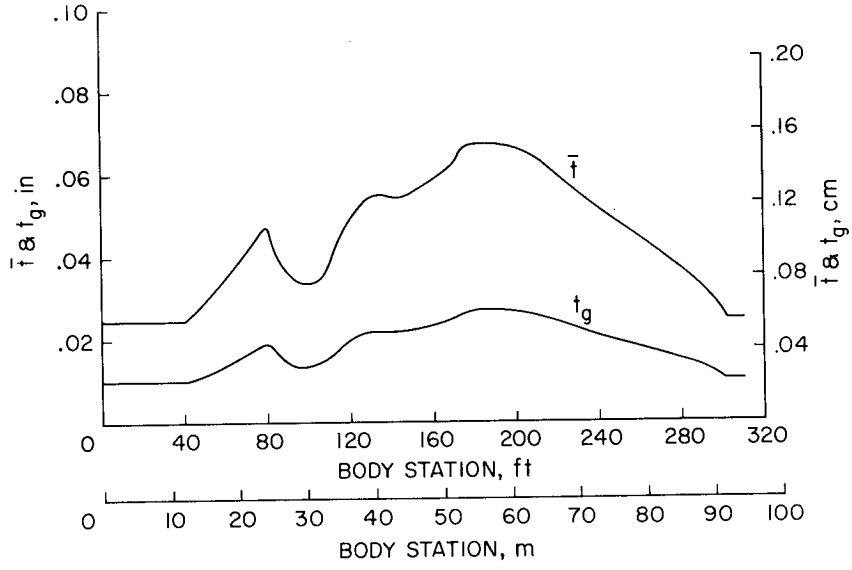

(a) Advanced.

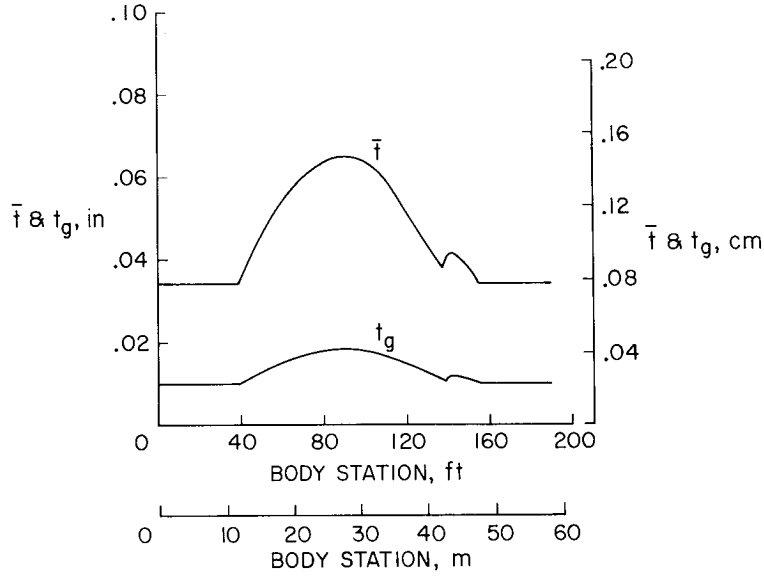

(b) Potential.

Figure 6.– Shell thicknesses.

The weight breakdowns of the two nominal concepts are shown in figure 7, where both weight fractions (of gross weight) and absolute weights are given. The load-carrying body structure weight consists of a shell, frames (stiffened shell concepts only), walls or truss work (all-body integral tankage concepts only), spanwise stiffening (all-body concepts only), and nonoptimum weight. Walls or truss work is used to carry pressure loads in the all-body integral tankage designs because this type of construction is more efficient than a shell. As previously mentioned, spanwise stiffening is required at the rear of all-body configurations because of the large span in that part of the vehicle. Designs with nonintegral tankage include tank weight; those with wing-body configurations include wing weight. The thermal protection system (TPS) weight includes insulation and, for cold structure concepts, the cover panels shown in figure 2. Most of the other items making up the dry weight of hypersonic aircraft (such as landing gear, control surfaces, fixed equipment, and propulsion system) vary only slightly with changes in vehicle concept and total about 25 percent of the gross takeoff weight for most designs. Weight statements of hypersonic vehicles may be found in references 10 and 11. In this paper, the term weight fraction refers only to those items shown on figure 7.

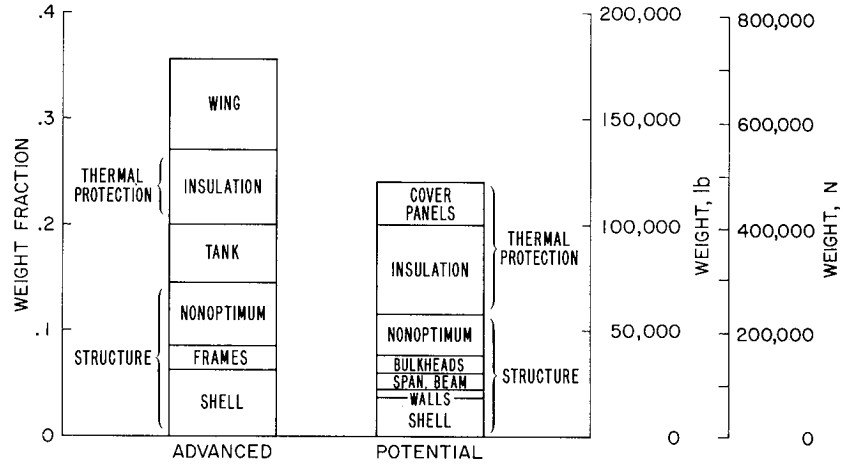

Figure 7.– Weight breakdown.

Note that the weight fraction of the potential concept, 0.240, is significantly less than that of the advanced, 0.355. The relatively low weight fraction of the potential concept is due primarily to the use of cold, integral tank structure as discussed later. The combined weight of the wing and tank required by the advanced concept more than account for its greater weight fraction. It is also of interest to note that the structure and TPS weight fractions are equal for the potential concept. Finally, it must be kept in mind that the potential concept, being a radical departure from conventional aircraft designs, contains many more design uncertainties than the advanced.

Effect of Variations in Shape and Size

The advanced concept– Figures 8, 9, and 10 show the effects of changes in three shape parameters on weight fractions; the tick marks on these figures indicate the nominal values of these parameters. The nominal shape analyzed here is not necessarily optimum; it was chosen only as a base about which shape variations were made.

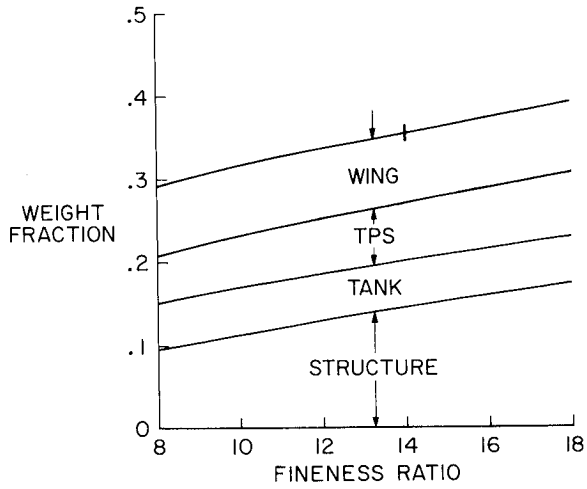

Figure 8.– Effect of fineness ratio (advanced).

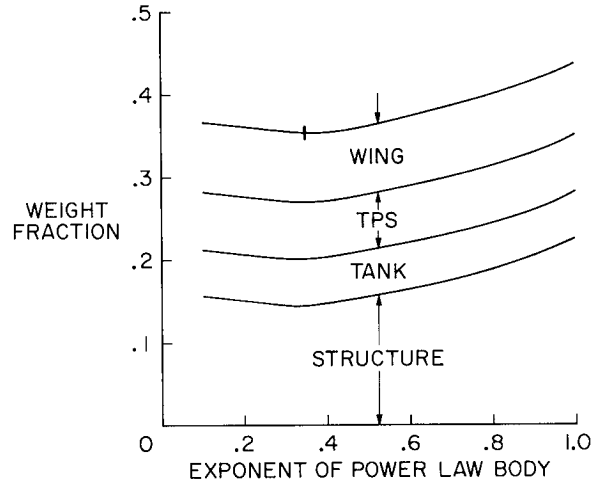

Figure 9.– Effect of exponent (advanced).

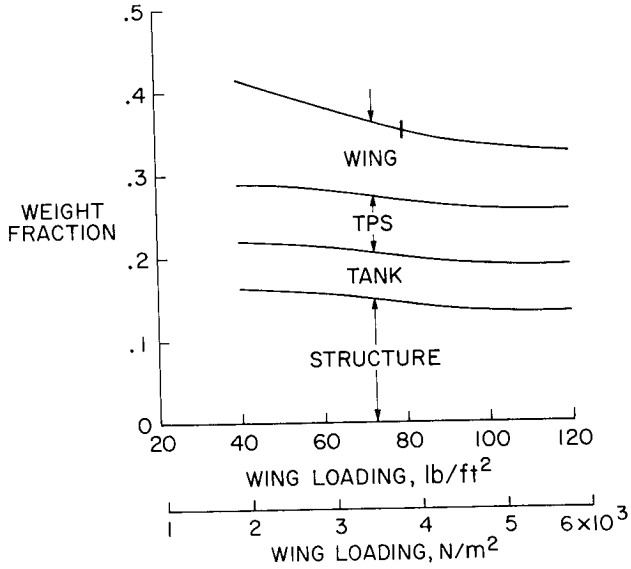

Figure 10.– Effect of wing loading (advanced).

Figure 8 shows the effect of variation of fineness ratio on the weight fraction. For this parameter, wing weight and tank weight remain fixed and the TPS weight increases slightly due to increasing surface area. With fineness ratio, however, body structure weight increases nearly linearly. Fineness ratio also has a strong and opposing influence on aerodynamic efficiency and is thus an important parameter for configuration optimization.

Figure 9 shows the variation of weight fraction with the exponent of the power law that defines body shape (appendix A). The shape varies from a cylinder (exponent = 0) to a double-ended cone (exponent = 1). The wing, TPS, and tank weights remain essentially constant for this variation. Since the maneuver loads decrease with increasing exponent (because the longitudinal lift and weight distribution becomes more similar) and the landing loads increase (because the vehicle length increases), the structural weight fraction has a minimum value at about the nominal value of the exponent.

The effect of varying takeoff wing loading is shown in figure 10. The predominant effect of increased wing loading (decreasing wing area) on the body structure is that the body carries an increasingly large percentage of the lift. As a result longitudinal lift and weight distributions are more compatible, thus reducing maneuver loads and hence structural weight. The TPS and tank weights remain constant, while the wing weight decreases as wing loading increases. The net effect is a significant decrease in weight fraction with increasing wing loading. In practical designs, this increase in wing loading is limited by landing and takeoff considerations, cruise efficiency, strength of sonic boom, and so on.

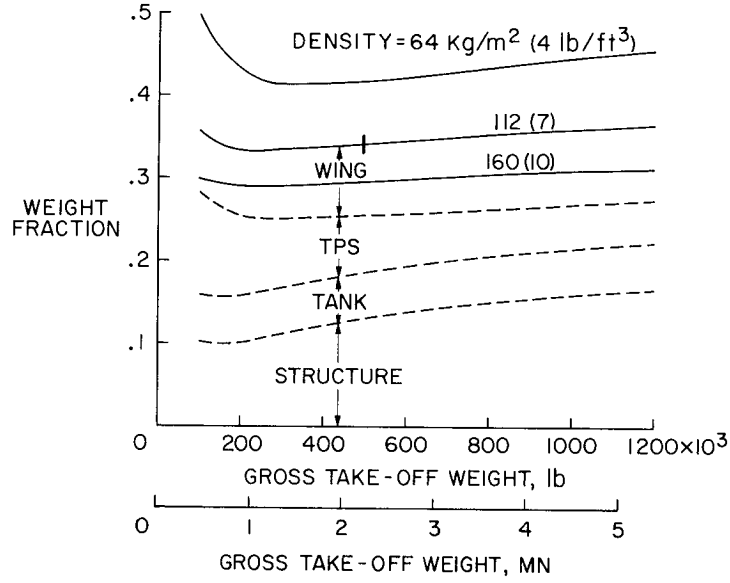

Figure 11.– Effect of size (advanced).

Figure 11 shows the effect of size on the weight fraction of the advanced concept; the tick mark indicates the gross weight and density of the nominal design. The shape parameters R_{fin}, p, and W/S were held at their normal values, and only maneuver loads were considered. The three values of gross vehicle density examined cover the range of possibilities for LH_2 fueled, hypersonic vehicles; because of the low density of hydrogen fuel (about 72 kg/m^3 (4–1/2 lb/ft^3)), these values are lower than those typical of current transport aircraft (about 160 to 400 kg/m^3 (10 to 25 lb/ft^3)). Individual weight items are shown only for the 112 kg/m^3 (7 lb/ft^3) density, but the variations seen here typify results for other densities.

As would be expected the body structure weight fraction increases with gross takeoff weight (W_{TO}), except at low gross weights where the structure is significantly affected by the minimum gage constraint. It is also evident that the variation of structure weight fraction with W_{TO} agrees well with the relationship $(W_{BS}/W_{TO}) \sim W_{TO}^{1/6}$ obtained by combining the simplified bending moment versus gross takeoff weight relationship of reference 13 with the assumption that the entire structure is buckling limited. Tank weight fraction for this design is independent of W_{TO} for constant density because tank weight is assumed to scale linearly with body volume. The TPS weight fraction, which is predominantly influenced by surface area, increases as W_{TO} decreases, and it assumes major importance at low W_{TO} where the surface area to volume ratio is large. Wing weight fraction remains very nearly constant. The combined effect of all these variations produces a total weight fraction that is relatively insensitive to changes in W_{TO}, except at low values of W_{TO} where increases in TPS weight and, to a lesser extent, structure weight, result in higher weight fractions. Changes in density (hence also volume and surface area) affect the weight fraction primarily through TPS weight which, to a good approximation, is proportional to surface area. Lower density vehicles (larger volumes) are seen to have higher weight fractions.

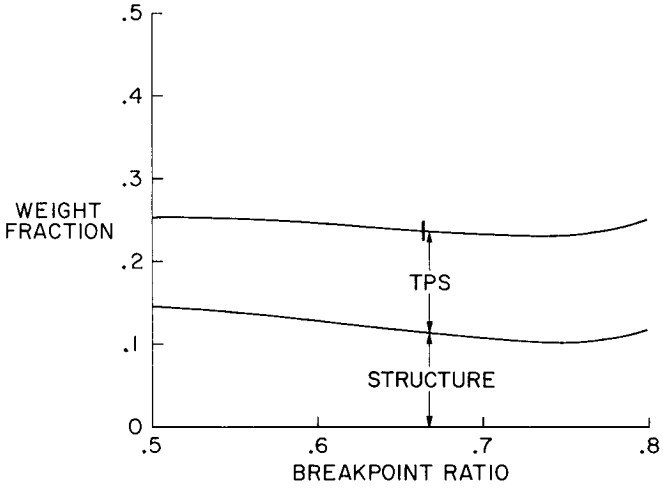

Figure 12.– Effect of breakpoint ratio (potential).

The potential concept– The effects of shape and size variations on the weight fractions of this concept are shown in figures 12 through 15; as before, the tick marks indicate the nominal values of the shape parameters. The effects of parametric variations on aerodynamic efficiency are discussed in reference 30. The effect of

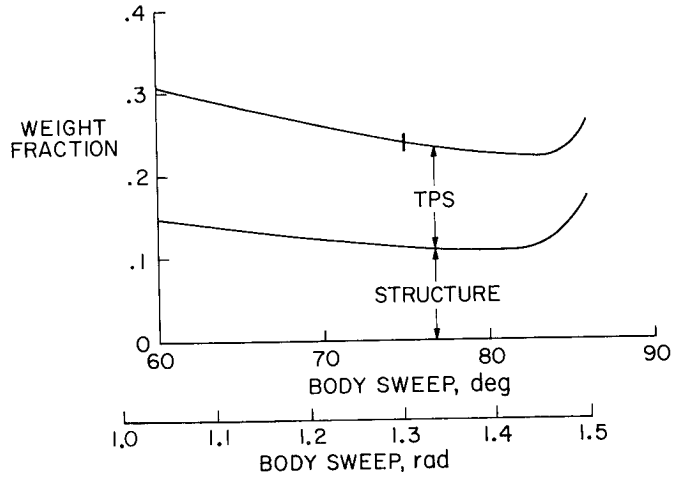

Figure 13.– Effect of body sweep.

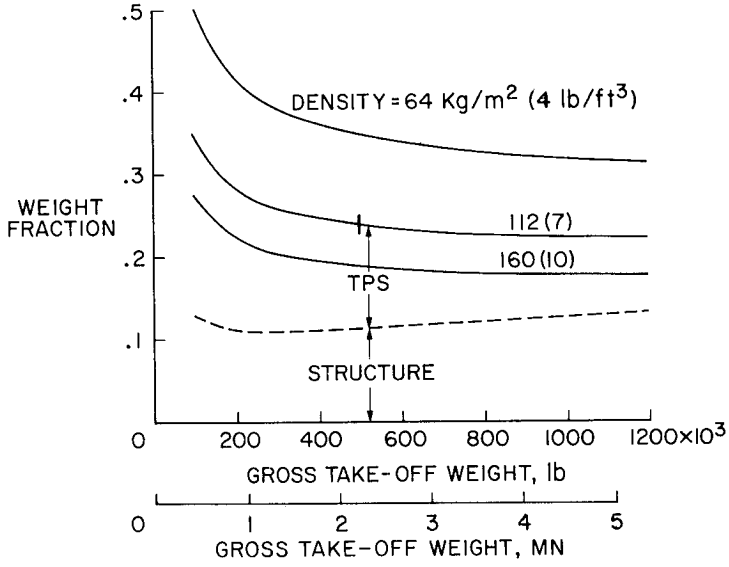

Figure 14.– Effect of fatness ratio.

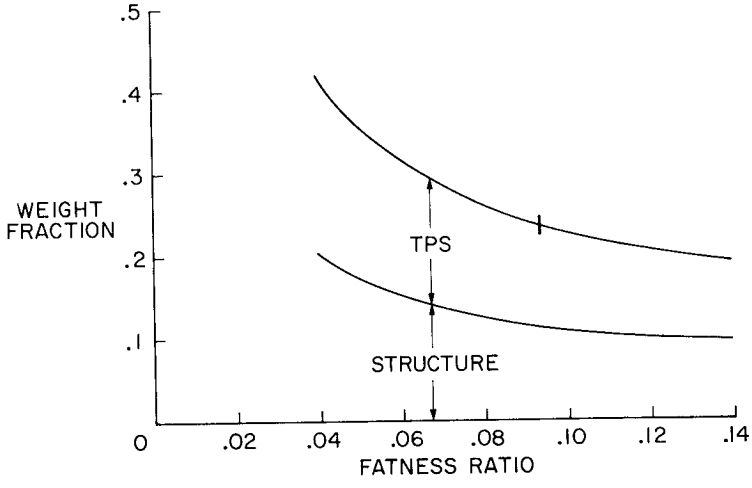

Figure 15.– Effect of size (potential).

breakpoint ratio (eq. (A9)) is shown in figure 12. Note that structural weight fraction tends to decrease as the breakpoint moves aft, while the TPS weight fraction tends to increase. The net effect of these two opposing influences results in a weight fraction that is fairly insensitive to breakpoint ratio.

Figure 13 shows that as the body sweep increases, structure weight fraction tends to decrease because the cross-sectional shape becomes increasingly cylindrical. The TPS weight fraction also decreases, primarily because of decreasing surface area. At sweeps approaching the limiting value of $\pi/2$ rad (90°), however, this trend is reversed due to the rapidly increasing vehicle length and associated increased structural weight. The overall result is the occurrence of a minimum value of weight fraction at about 1.4–1.5 rad (80°–85°) sweep.

The effect of varying fatness ratio (eq. (A8)) is shown in figure 14. As fatness ratio increases, the vehicle becomes more cylindrical and compact, causing both the structure and TPS weight fractions to decrease. It is apparent that the total weight fraction is very sensitive to this parameter, with large fatness ratios corresponding to low weight fractions. However, reference 30 shows that aerodynamic efficiency decreases sharply with increasing fatness ratio; this parameter therefore exerts great influence in configuration optimization.

Figure 15 shows the effect of size on the weight fraction of the potential concept for the same three densities considered for the advanced concept.

As before, only maneuver loads are considered, and the shape (R_{BR}, R_{fat}, Λ) is held fixed. Comparing figures 11 and 15, the structure and TPS weight fraction variations with W_{TO} are evidently very similar for both concepts. For the potential concept, however, the relatively high TPS weight fraction compared to the structure weight fraction results in a reversal in weight fraction variation; the weight fraction decreases with increasing W_{TO}, and tends to approach a constant value as W_{TO} increases. This increase in weight fraction at low values of W_{TO} results primarily from the relatively large surface areas and minimum gage restrictions on the structure accompanying the reductions in overall sizes. Simplified analysis gives the relationship $(W_{BS}/W_{TO}) \sim W_{TO}^{1/5}$ which agrees reasonably well with figure 15. The effect of density on the weight fraction is the same as for the advanced concept. Reference 30 indicates that aerodynamic efficiency is relatively insensitive to variations in size for the potential concept.

Effect of Variations in Design Criteria and Mission Requirements

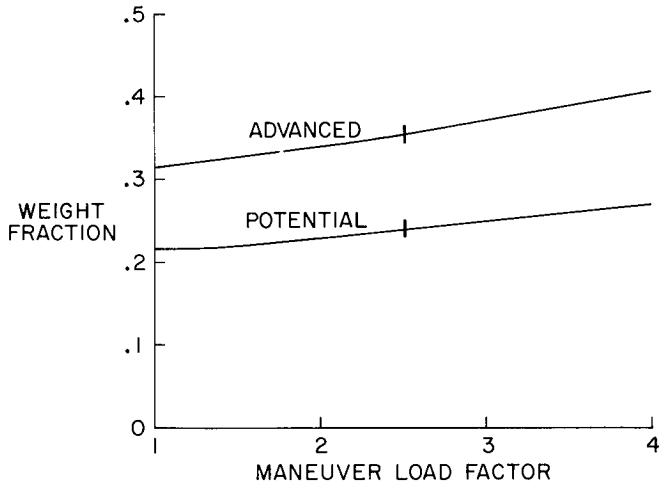

Figure 16.– Effect of load factor.

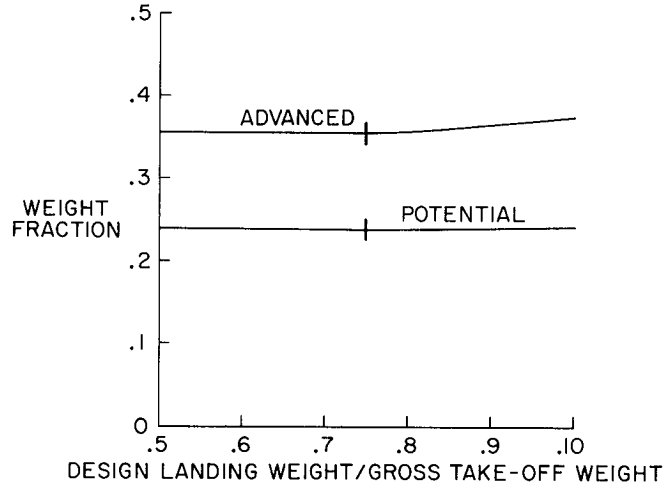

Figure 17.– Effect of design landing weight.

The effect of load factor n is summarized in figure 16 for both concepts. Tank weights was held constant and TPS weight remained nearly constant. Both wing weight and body structure weight, however, increased with increasing load factor, thereby causing total weight fractions of both concepts to increase. The weight fraction increase is very nearly linear above about $n = 2$; below this value, both landing and maneuver loads influence the design.

Figure 17 shows the effect of design landing weight. Only body structure weight is affected by this parameter. The weight fractions of both concepts are seen to be relatively insensitive to this parameter even for values approaching the gross takeoff weight. It may be concluded, therefore, that the weight penalty incurred by the requirement that these particular vehicles land at gross takeoff weight will be small.

One of the most important mission parameters for hypersonic cruise vehicles is cruise Mach number M_C. Before discussing the effect of M_C variations on weight fraction, it is instructive to consider the temperature-time characteristics of hypersonic cruise aircraft. Typical plots of temperature and time as a function of cruise Mach number for a fixed

range are shown in figure 18 (ref. 30). The cruise time t decreases in an asymptotic fashion as M_C increases, while surface temperatures increase. The maximum exterior surface temperature T_{struc} is used for computation of hot structure and cover panel weights, while the mean upper and lower surface temperatures $\bar{T}_{upper}$ and $\bar{T}_{lower}$ are used in the computation of insulation weight. To a first approximation, insulation unit weight is proportional to the rectangular temperature-time pulse (area under the T versus t curve; ref. 27). Since figure 18 indicates that the products $\bar{T}_{upper} \times t$ and $\bar{T}_{lower} \times t$ are very nearly independent of M_C, it can be expected that insulation weight will be fairly insensitive to M_C.

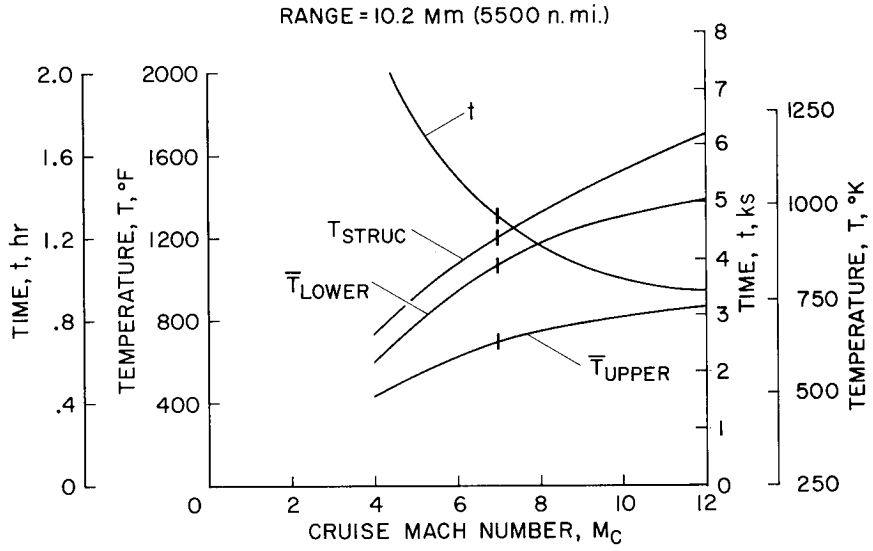

Figure 18.– Temperature-time characteristics.

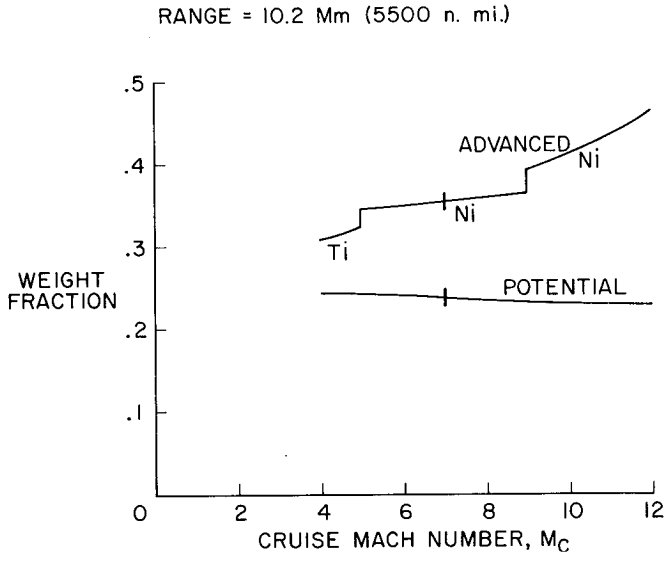

Figure 19.– Effect of cruise Mach number.

From data in figure 18 the effect on weight fraction of cruise Mach number M_C is shown in figure 19 for both nominal concepts at a fixed range of 10.2 Mm (5500 n. mi.). For the advanced concept, the tank weight remains constant for this variation, and the TPS weight, for reasons discussed above, remains very nearly constant. The wing and body structure weights increase with M_C because they are exposed to the increasing exterior surface temperature. Titanium alloy structure appears best for cruise Mach numbers up to about 5, at which point loss in ductility of present day alloys due to thermal effects prohibits further use. A high-strength nickel alloy is applicable for vehicles in the Mach number range of 5 to 9, while a lower strength nickel alloy with better oxidation resistance is required above about Mach 9.

The trend for the advanced concept is obviously increasing weight fraction with increasing M_C. The trend of the potential concept, however, is quite different. In this design, the body structural temperature (and hence the weight) is held fixed, and the TPS weight varies as the exterior temperatures and time vary. Since TPS weight is insensitive to M_C (assuming cover panel weight does not change radically), the potential concept weight fraction is very nearly independent of cruise Mach number and, in fact, decreases slightly at higher M_C. More generally, it would appear that the weight fraction of any vehicle with cold integral tankage flying a fixed range mission will be insensitive to M_C, regardless of vehicle configuration. The comparison of the two concepts in figure 19 shows that the potential concept becomes relatively lighter as M_C increases.

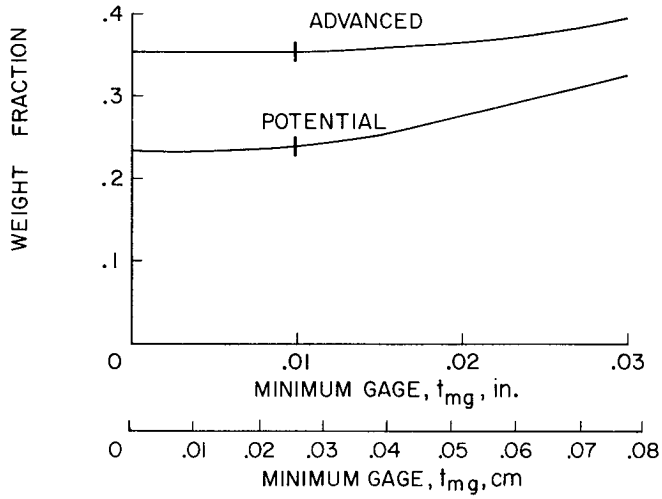

Figure 20.– Effect of minimum gage.

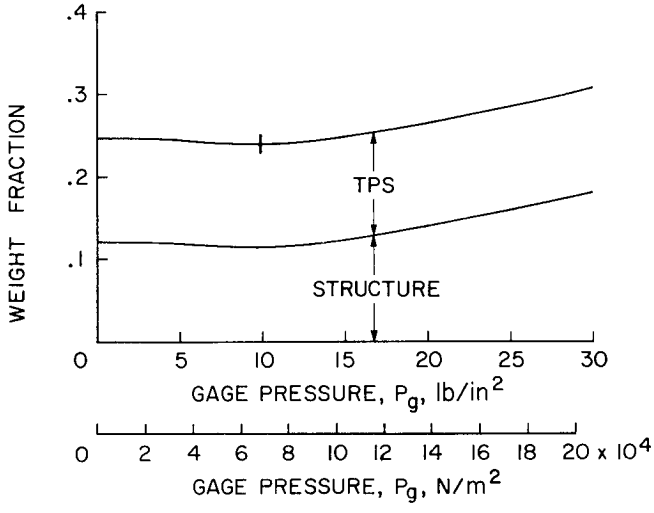

Figure 21.– Effect of pressurization (potential).

Since it was found that minimum gage t_{mg} restrictions on the body structure influence portions of the structure, the effect of minimum gage was investigated; the results are shown in figure 20. As might be expected the integrally stiffened shell of the advanced concept is less sensitive to t_{mg} than the sandwich shell of the potential concept. For the advanced concept, values of t_{mg} up to the nominal value of 0.0254 cm (0.01 in.) do not cause any significant increase in weight fraction. Above this value, the effect of t_{mg} becomes increasingly more significant until, at about 0.0762 cm (0.03 in.), the entire structure is minimum gage limited. For the potential concept, the minimum gage constraint has a slight but noticeable effect on the weight fraction at the nominal value. Above this value this constraint rapidly becomes significant with the entire structure being minimum gage at about t_{mg} = 0.0508 cm (0.02 in.)

For a pressure-stabilized, integral tank, cold structure there are two parameters that may be used for weight fraction minimization – internal gage pressure of the structure P_g and maximum allowable structural temperature. Figure 21 shows the effect of P_g on the weight fraction of the potential concept, in which pressure loads are used to relieve compressive loads. The weight initially decreases with P_g until a minimum weight is reached at the nominal pressure of about 69,000 N/m^2 (10 lb/in.^{2}); above this value, weight increases with pressure. The weight variation is seen to be slight up to pressures of about 103,500 N/m^2 (15 lb/in.^{2}).

The second of the two design parameters available for weight minimization is the maximum allowable structural temperature, which may be adjusted by varying insulation thickness. With increased structural temperature, body structure weight increases due to degradation in material properties, while the TPS weight decreases. The net effect (fig. 22) is that the weight fraction of the potential concept is independent of maximum structural temperature over a wide range of temperatures (about 367° K to 589° K (200° to 600° F)).

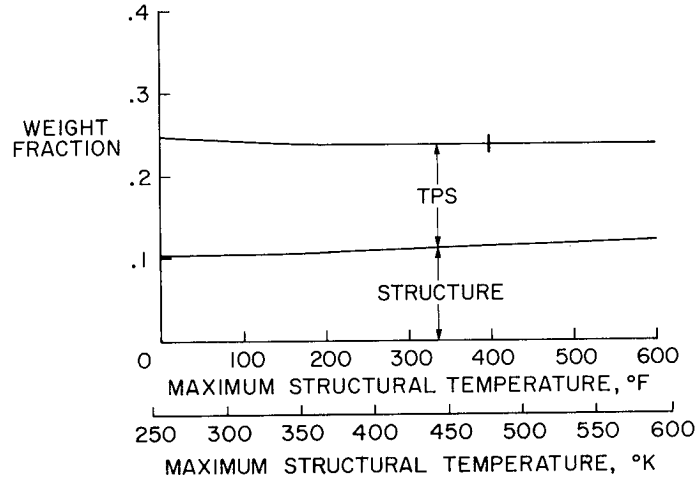

Figure 22.– Effect of structural temperature (potential).

Effects of Variation in Structural Concept

The last variation considered is the highly important one of structural concept. Considering the wing-body configuration first, figure 23(a) shows the weight fractions for four different structural concepts or designs. The first is the advanced concept already discussed. The second concept differs from the first in that insulation and cover panels are added to limit maximum

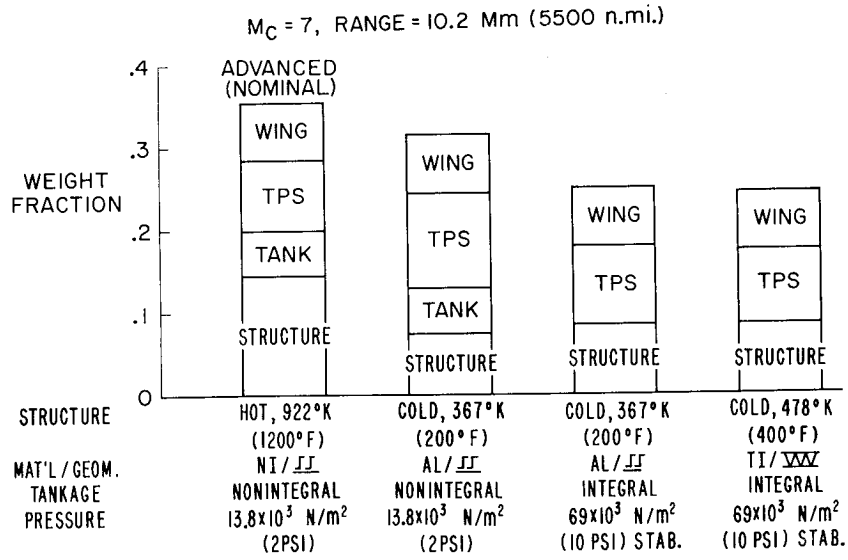

(a) Wing-body configuration.

Figure 23.– Effect of structural concept.

structural temperature to 367° K (200° F), thus permitting the use of an aluminum alloy, rather than a nickel alloy, structure. The results show that the decrease in structure weight (about 50 percent) more than compensates for the increase in TPS weight, and a significant reduction in total weight fraction is achieved. The third concept differs from the second in that pressure-stabilized, integral tankage is used. Even though pressure stabilization reduces structural weight slightly, this reduction is offset by the addition of bulkheads and other secondary structure required with integral tankage, and the structure weight fraction increases. A major improvement however, accrues from the elimination of the tank, enough so, in fact, that the total weight fraction of this concept is markedly lower than the previous one. In the fourth concept the aluminum structure is replaced with a titanium truss-core sandwich structure and sufficient thermal protection to limit maximum temperatures to 478° K (400° F). This change provides practically no improvement in the weight fraction. It is concluded from this figure that cold structure, integral tank designs are potentially lighter in weight than hot structure, nonintegral tank designs. For these lighter weight designs, the wing, TPS, and structure weights contribute approximately equally to the total weight. It must be remembered, however, that design complexity and development uncertainty tend to increase from left to right in figure 23(a).

Figure 23(b) presents the results of a similar analysis of the all-body configuration for the same four structural concepts. For this configuration it was found that the hot structure with nonintegral tank concept has a structure weight fraction of 0.71 and a total weight fraction of 0.86. This prohibitively high weight is due to pressure bending of the elliptical frames, which cannot be relieved by tension ties when a nonintegral tank is used. Even if the structure is aluminum alloy at 367° K (200° F) (the second concept on fig. 23(b)) the weight fraction is still a prohibitively high 0.61. It is clear that unsupported elliptical shells having ellipse ratios a/b approximating 4, when subjected to pressures even as small as 13,800 N/m^2 (2 psi), are impractical for hypersonic aircraft

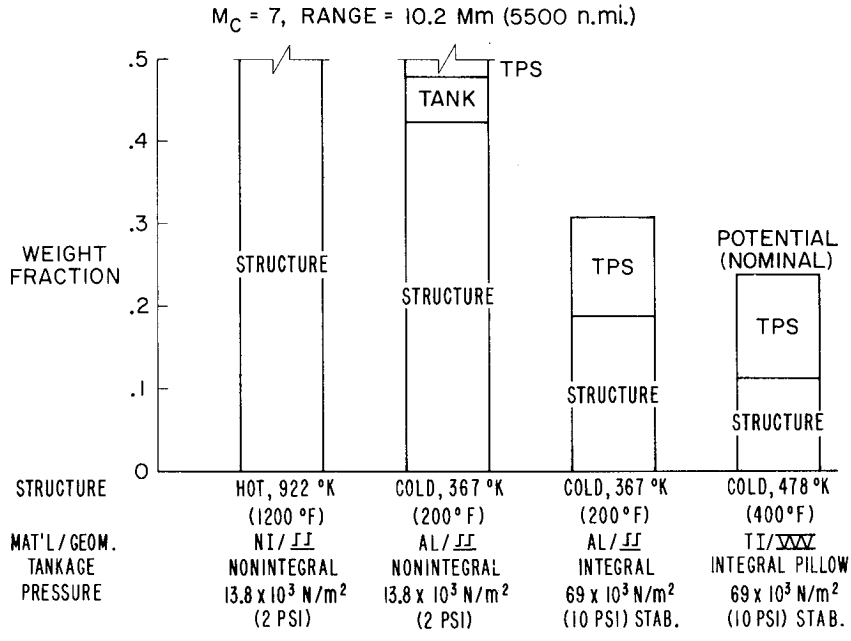

(b) All-body configuration.

Figure 23.– Concluded.

body structures. If pressure-stabilized, integral tankage structure with internal tension ties is used, the third concept in figure 23(b), a reasonable weight fraction results. The fourth concept, the potential concept discussed earlier, is significantly lighter than the third one.

Comparing figures 23(a) and (b) to assess the relative weights of the wing-body and the all-body configurations shows that for all structural concepts both the structure and TPS weight fractions are less for the wing-body than for the all-body. This is due primarily to the noncircular cross section of the all-body and its relatively high surface area. For the lighter weight designs, however, the advantage of the wing-body structure is offset by the wing weight, and both configurations have approximately the same weight fraction. The potential concept clearly is the lighter of the two concepts because it uses cold, integral tank structure – not because of its all-body configuration.

CONCLUDING REMARKS

The weight fractions of major structural components of hypersonic aircraft have been estimated for two nominal vehicle concepts. The advanced concept was found to have a structural weight fraction (consisting of body structure, body thermal protection system, tankage, and wing structure) of about 0.35. The potential concept had an equivalent weight fraction of about 0.24 with approximately half the weight in body structure and half in thermal protection system. The body structures of each concept were predominantly buckling critical with small portions limited by a minimum gage restriction.

For the advanced concept, fineness ratio was the shape parameter with the most influence on the weight fraction, while fatness ratio was the most influential for the all-body. As gross takeoff weight increases the structural weight fraction increases and the thermal protection weight fraction decreases. As a result, the total weight fraction increases slightly as gross takeoff weight increases in the case of the advanced concept, and decreases for the potential concept. At very low gross takeoff weights the weight fractions of both concepts become large. More dense vehicles were found to have lower weight fractions.

In the area of design criteria, it was found that weight fraction varied linearly with design maneuver load factor but was not affected by changes in design landing weight. Increasing the cruise Mach number for a constant range mission was found to increase the weight fraction of the advanced concept, while for the potential, the weight fraction did not vary significantly with Mach number. This conclusion appears to apply to any hypersonic aircraft with integral tankage for a fixed range mission. Although the potential concept was found to be more sensitive to minimum gage constraints than the advanced, this result was not significant for either concept. For pressure-stabilized, integral-tankage designs, the weight fraction appears to be relatively insensitive to design gage pressure, and to maximum structural temperature over a wide range of temperatures as well.

It was also determined that in general, cold structure designs are lighter than hot, and that pressure-stabilized, integral-tank structures are lighter than nonintegral. The lighter weight structures however, are also those involving the greatest design uncertainties. For the lightest weight

designs, concepts using wing-body configurations had about the same total weight fractions as those using all-body configurations. Vehicle designs involving hot, nonintegral structures and all-body configurations were found to be prohibitively heavy.

National Aeronautics and Space Administration
Moffett Field, Calif. 94035, October 5, 1971

APPENDIX A

VEHICLE GEOMETRIES

Considering the wing-body configuration first, the wing-loading gross density, and fineness ratio are defined as

$$W/S = W_{TO}/S_p \tag{A1}$$

$$\rho_B = W_{TO}/V_B \tag{A2}$$

$$R_{fin} = \ell/D \tag{A3}$$

where S_p is the wing plan area (see fig. 24). The body exterior contour is described by a power law as shown in the figure. A simple integration gives the body volume as

$$V_B = \pi D^2 \ell/4(2p + 1) \tag{A4}$$

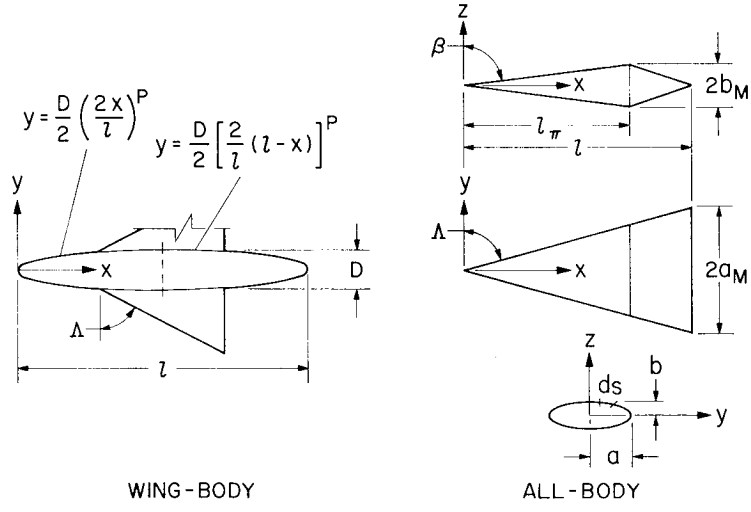

Figure 24.– Vehicle geometries.

Solution of equations (A2), (A3), and (A4) for the length ℓ results in

$$\ell = [4(2p + 1)R_{fin}^2 W_{TO}/\pi\rho_B]^{1/3} \tag{A5}$$

Thus, if the wing shape parameters Λ and W/S, the body shape parameters p and R_{fin}, and the body size parameters ρ_B and W_{TO} are all specified, the wing-body configuration is geometrically defined. A wing with leading edge sweep Λ of 1.22 rad (70°) was used throughout the study. Since the cross section of this configuration is circular, the cross section properties are well known.

For the all-body, the geometry is somewhat more complex because the lifting surface may not be sized independently of the body. The wing loading, gross density, fatness ratio, and breakpoint ratio are defined as

$$W/S = W_{TO}/S_p \tag{A6}$$

$$\rho_B = W_{TO}/V_B \tag{A7}$$

$$R_{fat} = S_\pi/S_p \tag{A8}$$

$$R_{BR} = \ell_\pi/\ell \tag{A9}$$

where S_p is the body plan area and S_π is the cross-sectional area at the breakpoint (S_π is also the maximum cross-sectional area if $0.5 < R_{BR} < 1.0$). With the aid of figure 24, the body plan area, breakpoint cross-sectional area, and volume are computed to be

$$S_p = \ell^2/\tan\Lambda \tag{A10}$$

$$S_\pi = \pi\ell_\pi^2/\tan\Lambda\tan\beta \tag{A11}$$

$$V_B = \pi\ell_\pi\ell(\ell + \ell_\pi)/6\tan\Lambda\tan\beta \tag{A12}$$

Inspection of equations (A6) through (A12) shows that the all-body geometry will be defined if the shape parameters Λ, R_{fat}, and R_{BR} and the size parameters ρ_B and W_{TO} are specified. Expressing the length in terms of these parameters gives

$$\ell = [6R_{BR}W_{TO}\tan\Lambda/(1 + R_{BR})R_{fat}\rho_B]^{1/3} \tag{A13}$$

so that the length of the all-body scales with $(W_{TO}/\rho_B)^{1/3}$ for constant shape. The wing loading of this configuration in terms of the configuration parameters is

$$\frac{W}{S} = \left[\frac{W_{TO}(1 + R_{BR})^2 R_{fat}^2 \rho_B^2 \tan\Lambda}{36R_{BR}^2}\right]^{1/3} \tag{A14}$$

This relation is plotted for the nominal shape in figure 25. The ellipse ratio a/b of the forebody is given by

$$a/b = \pi R_{BR}^2 \cot\Lambda/R_{fat} \tag{A15}$$

The section properties of elliptical shells will be needed for the weight analysis. The cross-sectional area and perimeter are given by

$$A = \pi ab \tag{A16}$$

$$P = 4aE_{II} \tag{A17}$$

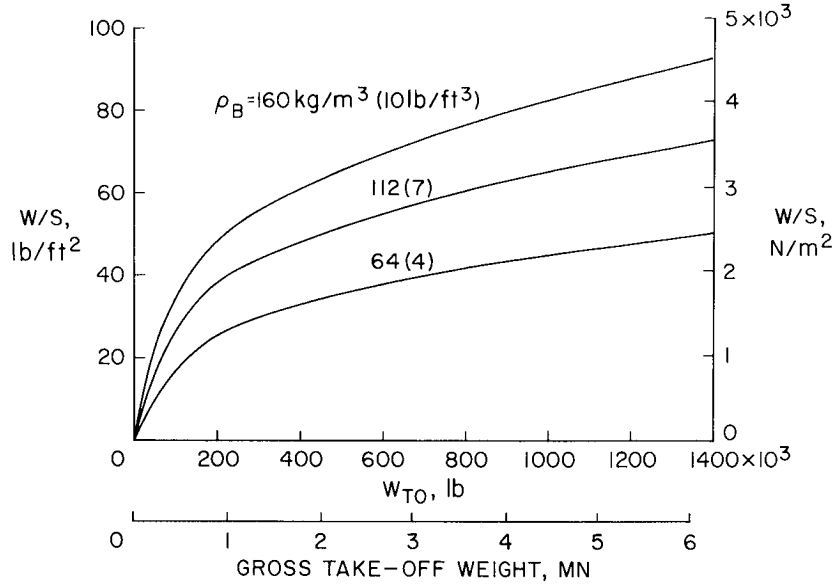

Figure 25.– Wing loading (all-body configuration).

The moment of inertia about the y axis divided by the shell thickness is found from

$$I'_y = \frac{I_y}{t_s} = 4\int_0^a z^2\, ds$$

$$= 4\int_0^a \left(1 - \frac{y^2}{a^2}\right) b^2 \sqrt{1 + \frac{b^2 y^2}{a^2(a^2 - y^2)}}\, dy$$

$$= 4ab^2\left[E_{II} - \left(\frac{2E_{II} - E_I}{3}\right) - \left(\frac{E_I - E_{II}}{3e^2}\right)\right] \tag{A18}$$

where E_I and E_{II} are the complete elliptic integrals of the first and second kind, respectively, and where

$$e = \sqrt{1 - (b/a)^2} \tag{A19}$$

is the eccentricity. The following approximate expressions for P and I'_y were found to give good agreement with equations (A17) and (A18) for the values of e of interest:

$$P = 2\pi a\sqrt{1 - (e^2/2)} \tag{A20}$$

$$I'_y = (\pi/4)ab^2\,[3 + (b/a)] \tag{A21}$$

For concepts employing pillow tankage, the structure is not in the shape of the vehicle configuration but consists of intersecting cones fitted within the elliptical cross section of the all-body as shown in figure 26. The number of circular sections or lobes is taken to be the nearest odd integer to

$$N_T = 2(a/b) + 1 \tag{A22}$$

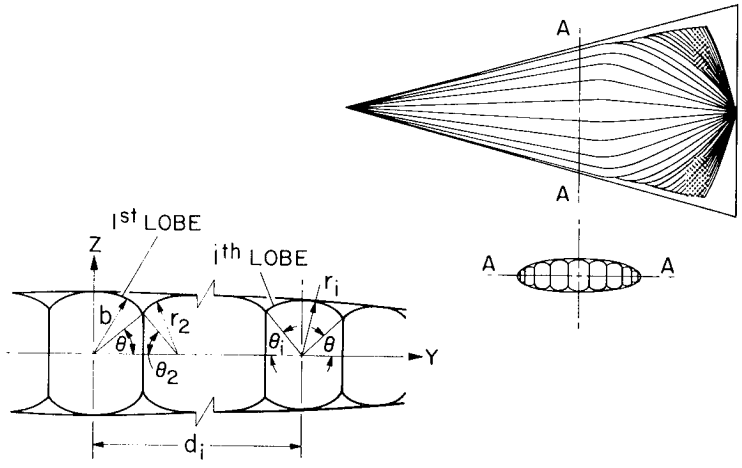

Figure 26.– Pillow tank geometry.

This relation was determined empirically and gives minimum or near minimum weight for the configuration variations considered in this study. Referring to figure 26, the equations defining the ith lobe in terms of the i – 1th are

$$e^2 r_i^2 = e^2 b^2 - d_i^2 \tag{A23}$$

$$r_i \sin \theta_i = r_{i-1} \sin \theta \tag{A24}$$

$$d_i - d_{i-1} + r_{i-1} \cos \theta + r_i \cos \theta_i \tag{A25}$$

where equation (A23) is the condition of tangency of the circle and the ellipse. These equations are solved sequentially at each body station x beginning with the center lobe. The free parameter θ is available for weight and volume optimization as discussed in appendix B. The perimeter, cross-sectional area, and I'_y of the circular lobes at any section are given by

$$P_s = 2\left[\pi b - 2b\theta + \sum_{i=2}^{N'_T - 1} (2\pi r_i - 2r_i\theta_i - 2r_i\theta) + 2\pi r_{N'_T} - 2r_{N'_T}\theta_{N'_T}\right] \tag{A26}$$

$$A = 2\left\{\frac{\pi b^2}{2} - \frac{1}{2}b^2(2\theta \sin 2\theta) + \sum_{i=2}^{N_T'}\left[\pi r_i^2 - \frac{1}{2}r_i^2(2\theta_i - \sin 2\theta_i) - \frac{1}{2}r_i^2(2\theta - \sin 2\theta)\right]\right.$$
$$\left. + \pi r_{N_T'}^2 - \frac{1}{2}r_{N_T'}^2\left(2\theta_{N_T'} - \sin 2\theta_{N_T'}\right)\right\} \tag{A27}$$

$$I_y' = 4\left[\frac{b^3}{2}\left(\cos\theta \sin\theta - \theta + \frac{\pi}{2}\right) + \sum_{i=2}^{N_T'-1}\frac{r_i^3}{2}(\cos\theta \sin\theta + \cos\theta_i \sin\theta_i + \pi - \theta - \theta_i)\right.$$
$$\left. + \frac{r_{N_T'}}{2}\left(\cos\theta_{N_T'} \sin\theta_{N_T'} + \pi - \theta_n\right)\right] \tag{A28}$$

where $N_T' = (N_T + 1)/2$. The perimeter of the vertical walls connecting the lobes is given by

$$P_W = 4 \sin\theta \sum_{n=1}^{N_T'-1} r_i \tag{A29}$$

A typical pillow tankage installation is shown in figure 26. In view of equation (A22), the forebody will have a fixed number of lobes while the number of lobes in the afterbody will increase toward the rear of the vehicle. This increase results in an afterbody structure that is an impractical design for an actual vehicle but is convenient for use in a mathematical model.

APPENDIX B

WEIGHT ANALYSIS

In this appendix, weight estimating methods are developed for the weight items considered in this study. Of primary concern is the structural analysis of the load carrying body structure. It is convenient to discuss the nonintegral and integral tankage cases separately. Weight estimation relationships of the other items (tank, thermal protection, and wing) are discussed briefly.

Body Structural Weight for Nonintegral Tankage Concepts

For all-body, nonintegral tankage concepts it has been found that pressure-induced bending loads of the elliptical shape tend to dominate longitudinal bending loads at the design pressure (13,800 N/m^2 (2 psi)) of nonintegral tankage structure. Since these pressure loads are best resisted by frames, only frame-supported, stiffened-shell structures will be considered for this concept. However, both frame-supported, stiffened-shell structures and sandwich-shell structures are applicable to wing-body, nonintegral tankage concepts. A separate tank weight is computed for nonintegral concepts.

Considering first the shell, the compressive and tension stress resultants in the axial direction x at a station x are

$$N_x^- = Mb/I_y' \tag{B1}$$

$$N_x^+ = (Mb/I_y') + (AP_g/P) \tag{B2}$$

respectively. The stress resultant in the hoop direction is

$$N_y = bP_gK_p \tag{B3}$$

where K_p is needed to account for the fact that not all of the shell material (e.g., core material in sandwich concepts) is available for resisting hoop stress. For the advanced and potential concepts, K_p is 2.48 and 3.41, respectively. Expressions for the geometrical quantities I_y', A, and P may be found in appendix A. The quantity b is replaced by r for wing-body concepts. As may be seen from equation (B1), the shell is not pressure stabilized. The equivalent isotropic thicknesses of the shell are given by

$$\bar{t}_{S_C} = N_x^- /F_{cy} \tag{B4}$$

$$\bar{t}_{S_T} = (1/F_{tu})\max(N_x^+, N_y) \tag{B5}$$

$$\bar{t}_{S_G} = K_{mg}t_{mg} \tag{B6}$$

for designs limited by compression, tension, and minimum gage, respectively. In equation (B6), t_{mg} is a specified minimum material thickness and K_{mg} is a parameter relating $\bar{t}_{S_G}$ to t_{mg} which depends on the shell geometry. For the advanced and potential concepts, K_{mg} is 2.48 and 3.41, respectively; t_{mg} is held at 0.0254 cm (0.01 in.) for both concepts. A fourth thickness that must be considered is that for buckling limited designs $\bar{t}_{S_B}$ is discussed in appendix C.

The elliptical frames of the all-body may be sized either by buckling, as described in appendix C, or by pressure bending. An expression for the "smeared" equivalent thickness, $\bar{t}_{F_P}$, required to preclude pressure bending will now be derived. Using the methods and nomenclature of reference 32 (sec. 81), the redundant bending moment at the ends of the semimajor axis (point of maximum bending stress) of an elliptical frame, due to an internal pressure, P_g, is

$$M_a = -\frac{\int^s M' ds}{\int^s ds} + P_g a^2 d$$

$$= -\frac{P_g d}{8 a E_{II}} \int_0^a \left[y^2 + b^2 + a^2 - \left(\frac{b}{a}\right)^2 y^2 \right] \sqrt{1 + \frac{b^2 y^2}{a^2 (a^2 - x^2)}}\, dx + P_g a^2 d$$

$$= -\frac{P_g d a^2}{6} \left(e^2 + 1 + \frac{e^2 E_I}{E_{II}} - \frac{E_I}{E_{II}} \right) \tag{B7}$$

The frame shape parameters are defined as

$$K_{F1} = I_F / A_F^2 \tag{B8}$$

$$K_{F2} = \sqrt{A_F} / d_F \tag{B9}$$

where I_F, A_F, d_F are the moment of inertia, cross-sectional area, and semidepth of the frame cross section. The values of K_{F1} and K_{F2} were held at 5.24 and 0.33, respectively, throughout the study. Using equations (B8) and (B9), the flexure formula gives

$$A_F = (M_a / K_{F1} K_{F2} F_{tu})^{2/3} \tag{B10}$$

Substitution of equation (B7) in (B10) and "smearing" the frames according to $A_F = \bar{t}_{F_P} d$ gives

$$\bar{t}_{F_P} = \left\{ \frac{P_g a^2 [e^2 + 1 + (e^2 E_I / E_{II}) - (E_I / E_{II})]}{6 K_{F1} K_{F2} F_{tu} \sqrt{d}} \right\}^{2/3} \tag{B11}$$

If relations (A17), (A18), (A20), and (A21) are used, this expression is closely approximated by

$$\bar{t}_{F_P} = \left\{ \frac{P_g a^2 e^2 [3 + (b/a)]}{16 K_{F1} K_{F2} F_{tu} \sqrt{d} \sqrt{1 - (e^2/2)}} \right\}^{2/3} \tag{B12}$$

which is the expression used in the analysis. For the circular cross section of the wing-body, $\bar{t}_{F_P} = 0$ as required. If the shell is buckling critical and the frames are pressure bending critical, the total equivalent thickness is

$$\bar{t} = \bar{t}_{S_B} + \bar{t}_{F_P} \tag{B13}$$

where $\bar{t}_{S_B}$ is given by equation (C2) and $\bar{t}_{F_P}$ by equation (B12). If equation (B13) is minimized with respect to d there results

$$\bar{t} = \frac{5}{3} \left\{ \frac{9 a^3 M P_g{}^2 e^4 [3 + (b/a)]}{16^2 \pi K_{F1}{}^2 K_{F2}{}^2 b E \epsilon F_{tu}{}^2 [1 - (e^2/2)]} \right\}^{1/5} \tag{B14}$$

$$\bar{t}_{S_B} = \frac{2}{5} \bar{t}$$

$$\bar{t}_{F_P} = \frac{3}{5} \bar{t}$$

$$d = \left\{ \frac{\pi^3 a^{11} b^3 e^8 [3 + (b/a)]^2 P_g{}^4 E^3 \epsilon^3}{4^3 16^4 K_{F1}{}^4 K_{F2}{}^4 [1 - (e^2/2)]^2 M^3} \right\}^{1/5} \tag{B15}$$

Hence the frame weight is 1–1/2 times the shell weight.

At each fuselage station x of the all-body configuration, the shell may be sized by compression, tension, minimum gage, or buckling, and the frames may be sized by general instability or pressure bending. The problem is then to find the least total thickness $\bar{t} = \bar{t}_S + \bar{t}_F$ as a function of d which satisfies the eight conditions resulting from the possible combinations of shell and frame criteria. (This may be viewed as a problem in nonlinear mathematical programming.) Six of these conditions are monotonically decreasing with respect to d while the two involving shell buckling have minimums as given by equations (B14) and (C13). The minimum total thickness $\bar{t}$ is obtained by a sequential search procedure. For wing body configurations employing stiffened shell concepts the procedure for determining $\bar{t}$ is similar except that there is no pressure bending of the frames and hence only four conditions need be considered. For wing-body sandwich shell concepts, the search procedure for $\bar{t}$ becomes simply

$$\bar{t} = \bar{t}_S = \max(\bar{t}_{S_C}, \bar{t}_{S_T}, \bar{t}_{S_G}, \bar{t}_{S_B}) \tag{B16}$$

where t_{S_B} is given by equation (C11). The gage thickness is then computed from $t_g = \bar{t}_S/K_{mg}$. The ideal body structural weight of all-body vehicles is obtained by summation as

$$W_I = 2\pi\rho \sum_{\substack{\text{body} \\ \text{length}}} \bar{t}_i a_i \sqrt{1 - (e_i^2/2)}\, \Delta x_i \tag{B17}$$

where quantities subscripted i depend on x. For the circular cross section wing-body this reduces to

$$W_I = 2\pi\rho \sum_{\substack{\text{body} \\ \text{length}}} \bar{t}_i r_i \Delta x_i \tag{B17'}$$

Thus W_I is the theoretical weight required to preclude failure of the body structure by yielding and buckling, subject to a minimum gage constraint.

The preceding analysis may be used to estimate the relative weights of elliptic and circular shells in bending. Consider an elliptical and a circular shell each of equal length and equal enclosed cross-sectional area. Let the structure of both shells be a frame-stabilized, integrally stiffened shell of the same material which is buckling critical, and suppose each shell to be loaded by the same bending moment (no pressure loading). Then, for the elliptical shell, equations (B17) and (C13) give

$$W_{I_{ellipse}} = \left(2\pi\rho a\sqrt{1 - \frac{e^2}{2}}\,\Delta x\right)\left\{\frac{4}{27^{1/4}}\left(\frac{\pi C_F}{K_{F1}\epsilon^3}\right)^{1/8}\sqrt{\frac{\bar{N}_x}{E}}\left[\sqrt{3 + \frac{b}{a}}\,(0.3719ab + 0.6281a^2)\right]^{1/4}\right\}$$

Setting r = a = b in this expression gives

$$W_{I_{circle}} = (2\pi\rho r\,\Delta x)\left[\frac{4}{27^{1/4}}\left(\frac{\pi C_F}{K_{F1}\epsilon^3}\right)^{1/8}\sqrt{\frac{\bar{N}_x}{E}}\,(2r^2)^{1/4}\right]$$

Using equation (B1) and setting $r = \sqrt{ab}$ the weight ratio is then

$$\frac{W_{I_{ellipse}}}{W_{I_{circle}}} = \left\{\left(\frac{a}{b}\right)^2\left(1 - \frac{e^2}{2}\right)^2\left[\frac{4}{3 + (b/a)}\right]^{3/2}\left(0.3719 + 0.6281\,\frac{a}{b}\right)\right\}^{1/4} \tag{B18}$$

This ratio, which is a function only of a/b, is plotted on figure 27. It is seen to be nearly linear; the elliptical shell being about twice as heavy as the circular one at a/b = 4. However, as mentioned earlier, pressure bending of the frames at the 13,800 N/m^2 (2 psi) design pressure dominates the frame sizing of the all-body in fuselage structure applications. If the shells are constructed of truss-core sandwich, equations (B17), (B1), and (C1) result in the ratio

$$\frac{W_{I_{ellipse}}}{W_{I_{circle}}} = \left(\frac{a}{b}\right)^2\sqrt{1 - \frac{e^2}{2}}\left\{\frac{4}{[3 + (b/a)]\,(a/b)^{3/2}}\right\}^{3/5} \tag{B19}$$

This ratio is also plotted in figure 27 and also varies nearly linearly with a/b but with a steeper slope. Since all-body configurations typically have a/b = 4 or greater it may be concluded, regardless of the structural concept used, that nonintegral all-body concepts are clearly prohibitively heavy as compared with wing-body concepts.

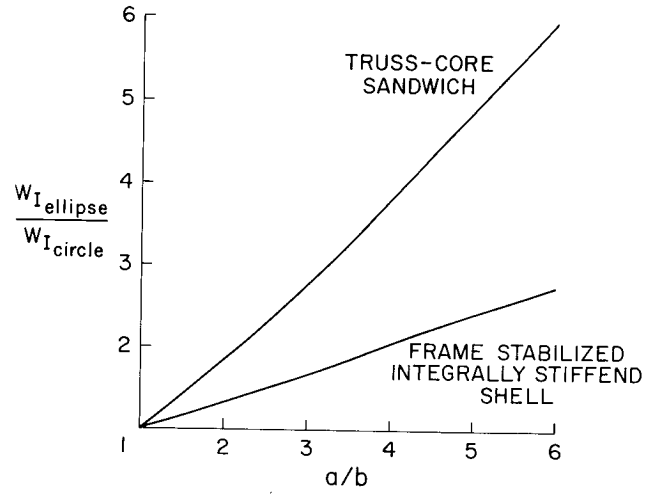

Figure 27.– Comparison of weights of unpressurized elliptic and circular shells.

The transverse bending moments associated with the large span of the rear portion of the all-body configuration require additional structure for this configuration. The weight of such structure was estimated by computing the weight of a spanwise beam capable of transmitting the horizontal tail loads into the body structure. The result obtained is

$$W_{SB} = 6\rho L_T a_M^2 / d_T F_{cy} \tag{B20}$$

where L_T is the vertical tail normal force at the design load factor, d_T is the beam depth (taken to be the body depth at the location of the tail), and a_M is the beam span (taken to be the body span at the location of the tail).

Body Structural Weight for Integral Tankage Concepts

Integral tankage concepts differ from nonintegral concepts in the manner in which they carry pressure loads and in the fact that the load-carrying body structure also serves as a fuel tank. For all-body configurations, a special structural concept called pillow tankage is considered.

Considering first elliptical shells, the stress resultants are the same as those derived in the preceding section, except that pressure stabilization is utilized, that is, N_x^- becomes

$$N_x^- = (Mb/I_y') - (AP_g/P) \tag{B21}$$

The shell thicknesses, $\bar{t}_{S_C}$, $\bar{t}_{S_T}$, $\bar{t}_{S_G}$, $\bar{t}_{S_B}$ are determined as before. For concepts employing the all-body configuration, internal tension ties are used to relieve the pressure bending stresses on the frames. Thus, frames are sized only by general instability for integral tankage. If the tension ties are sized by the hoop stress loads at the ends of the semimajor axis and "smeared," their equivalent isotropic thickness is given by

$$\bar{t}_T = AP_g/PF_{tu} \tag{B22}$$

The total thickness of the integral tankage concepts is then in the most general case

$$\bar{t} = \bar{t}_S + \bar{t}_F + \bar{t}_T \tag{B23}$$

where $\bar{t}_F = 0$ for sandwich shell structural concepts and $\bar{t}_T = 0$ for wing body concepts. The quantities $\bar{t}_S$ and $\bar{t}_F$ are obtained by a one parameter search that minimizes their sum in the same manner as was done for nonintegral tankage concepts. The ideal body structural weight is obtained from equation (B17). As before, for all-body configurations W_{SB} given by equation (B20) must be added to W_I. Also added to W_I for all integral tankage concepts is a tank weight which will be discussed later. These items are added before the nonoptimum factor is applied.

Because of the poor structural efficiency of pressure loaded elliptical shells, a special concept called pillow tankage is potentially attractive for all-body integral tankage concepts. This concept consists of a shell composed of intersecting cones fitted within the elliptical body. The geometry of pillow tankage is discussed in appendix A. The stress resultants on the circular lobes at the point of peak bending stress (ends of semiminor axis) are

$$N_{S_x}^{-} = (Mb/I_y') - AP_g/(P_S + P_W) \tag{B24}$$

$$N_{S_x}^{+} = (Mb/I_y') + AP_g/(P_S + P_W) \tag{B25}$$

$$N_{S_y} = bP_gK_p \tag{B26}$$

The maximum stress resultants on the vertical walls are

$$N_{W_x} = P_gA/(P_S + P_W) \tag{B27}$$

$$N_{W_z} = P_g(b\cos\theta + r_2\cos\theta_2) \tag{B28}$$

The equivalent isotropic thicknesses of the shell are given by

$$\bar{t}_{S_C} = N_{S_x}^{-}/F_{cy} \tag{B29}$$

$$\bar{t}_{S_T} = (1/F_{tu})\max(N_{S_x}^{+}, N_{S_Y}) \tag{B30}$$

$$\bar{t}_{S_G} = K_{mg} t_{mg} \tag{B31}$$

for designs limited by compression, tension, and minimum gage, respectively, and for the walls

$$\bar{t}_{W_T} = (1/F_{tu})\max(N_{W_x}, N_{W_z}) \tag{B32}$$

$$\bar{t}_{W_G} = K_{mg} t_{mg} \tag{B33}$$

for designs limited by tension and minimum gage. The shell thickness, $\bar{t}_S$, is determined as the least thickness which precludes failure by tension, compression, and buckling without violating minimum gage restrictions. The shell concept may be either frame-stabilized, integrally stiffened shell or sandwich shell. Buckling equations for these concepts are found in appendix C. The ideal structural weight of pillow tankage concepts is obtained by the summation

$$W_I = \rho \sum_{\substack{\text{body} \\ \text{length}}} (P_{S_i} \bar{t}_{S_i} + P_{W_i} \bar{t}_{W_i}) \Delta x_i \tag{B34}$$

where quantities subscripted i depend on x and where

$$\bar{t}_W = \max(\bar{t}_{W_T}, \bar{t}_{W_G}) \tag{B35}$$

The parameter θ (fig. 26) is available for vehicle performance optimization. The function $W_I(\theta)$ monotonically decreases within the range $0 < \theta < \pi/2$, and θ therefore should be as large as possible to minimize W_I. (Although it is possible for eq. (A22) to restrict the range of θ, this limitation was not encountered in this study.) However, as θ approaches $\pi/2$ the tank volume decreases (recall that the number of lobes, N_T, is fixed by eq. (A22)) and thus the volumetric efficiency η, defined as the ratio of tank volume to body configuration volume, must be considered as well as W_I. For the designs considered in this study, $\eta(\theta)$ is a concave downward function having a local maximum for some value of θ on $0 < \theta < \pi/2$. The payload performance of a hypersonic cruise vehicle, Φ, will be a function of both W_I and η, that is, $\Phi = \Phi(W_I, \eta)$; hence the rate of change of payload with respect to θ is

$$\frac{d\Phi}{d\theta} = \left(\frac{\partial \Phi}{\partial W_I}\right)_\eta \frac{dW_I}{d\theta} + \left(\frac{\partial \Phi}{\partial \eta}\right)_{W_I} \frac{d\eta}{d\theta} \tag{B36}$$

The necessary condition for maximum Φ gives to a first-order approximation

$$\left(\frac{\partial \Phi}{\partial W_I}\right)_\eta (W_{I_{opt}} - W_{I_o}) + \left(\frac{\partial \Phi}{\partial \eta}\right)_{W_I} (\eta_{opt} - \eta_o) = 0 \tag{B37}$$

where $(\partial\Phi/\partial W_I)_\eta$ and $(\partial\Phi/\partial\eta)_{W_I}$ are the sensitivities of payload to W_I at constant η and to η at constant W_I, respectively, and where W_{I_0} and η_0 are nominal values. Values of the partial derivatives are determined from a sensitivity study performed with a mission analysis program. Equation (B37) is solved for the optimum values $W_{I_{opt}}$ and η_{opt} using Newton's method with θ as the independent parameter. For the nominal potential concept vehicle, the above procedure gave $\theta = 0.94$ rad (54°).

Nonoptimum Body Structure Weight

Since the above analysis gives only the ideal weight, W_I, the "nonoptimum" weight (fasteners, cutouts, surface attachments, uniform gage penalties, manufacturing constraints, etc.) has yet to be determined. The method used here is explained with the aid of figure 28 which is a log-log plot of body weight as a function of a weight estimation parameter, χ, which accounts for the effects of gross weight, body dimensions and design load factor. The circles on the figure indicate body weights of existing aircraft; the lower line represents the equation developed in reference 3 to estimate body weight of wing-body hypersonic aircraft.

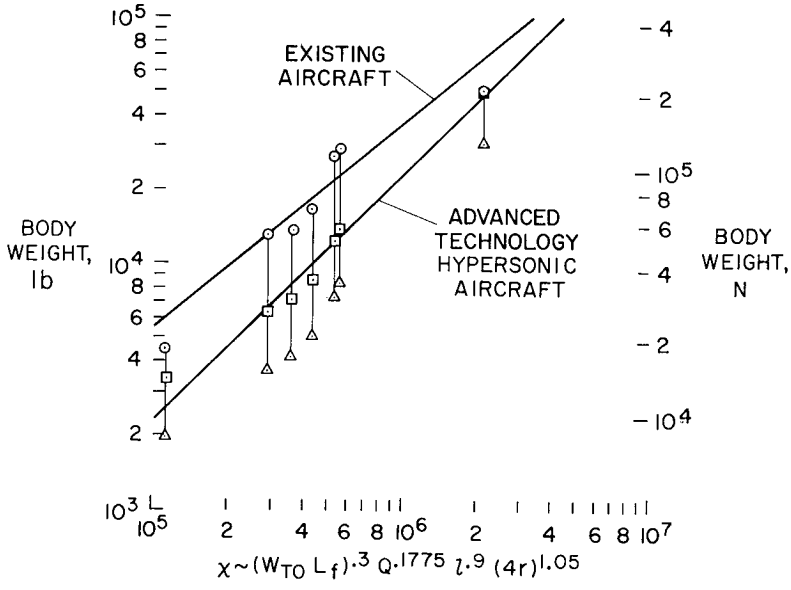

Figure 28.– Correlation and comparison of method of analysis.

The analysis developed in the present study was applied to the same existing aircraft and the resulting ideal weights are shown by the triangles. A two parameter regression analysis based on ideal weight, W_I, and body surface area, A_B, was then employed to obtain the best fit with the advanced technology hypersonic aircraft line. The resulting body weights are shown by the squares, and the total weight of the body structure is

$$W_{BS} = 1.64W_I + 3.8\ (0.08)A_B \tag{B38}$$

Equation (B38) was used for all vehicle concepts considered in this report. The correlation with existing aircraft is quite good (fig. 28) except for the aircraft at the extreme values of the weight

parameter. This conclusion is established by the fact that the scatter of the squares about the lower curve is in the same pattern as the scatter of the actual weights about the upper curve, which is a curve fit of these weights.

Tank, Thermal Protection, and Wing Weights

To a first approximation the weight of a circular fuel tank constructed of a given material and designed to a given pressure will scale linearly with tank volume. Thus for nonintegral tank concepts, the tank weight is estimated by

$$W_{TK} = 6.13\ (0.383)V_B \tag{B39}$$

where the constant of proportionality has been determined by using the weight of the tank described in reference 26 as a reference point, assuming, a nickel alloy tank designed for 105,500 N/m^2 (15.3 psig).

For integral tank concepts weight must be added to the ideal body structural weight, equation (B17), to account for bulkhead and other items necessary for containment of fuel. Since both the material and pressure will vary from design to design, the following equation is used

$$W_{TK} = 4720\ \frac{\rho P_g V_B}{F_{tu}} \tag{B40}$$

for these concepts, provided P_g is greater than atmospheric pressure. The functional dependence in this equation comes from a membrane analysis of a spherical tank. The numerical constant has been determined by using the bulkheads of the tank described in reference 26 as a reference point.

The weight of the body thermal protection system is estimated from

$$W_{TPS} = A_B(U_{CP} + U_{const} + K_{TPS}U_{ins}) \tag{B41}$$

In this equation U_{CP} is the unit mass (weight) of the cover panels, estimated to be 4.33 kg/m^2 (0.886 lb/ft^2) for the super alloys (temperature limit 1255° K (1800° F)) listed in reference 3, U_{const} is the mass (weight) of stand-offs and other items and is taken to be 1.16 kg/m^2 (0.238 lb/ft^2) from reference 26, and K_{TPS} is a nonoptimum factor taken as 1.286 for this study. The unit weight of the insulation plus boiloff, U_{ins} is computed from the transient analysis described in reference 27. The insulation system used in this calculation is helium-purged, quartz-fiber with a density of 56 kg/m^3 (3.5 lb/ft^3), pressurized at 300 mm of Hg. For the purposes of this calculation, $\overline{T}_{lower}$ from figure 18 was identified with $\overline{T}_{wet}$ in reference 27 and $\overline{T}_{upper}$ with $\overline{T}_{dry}$. It was assumed that the dry tank solution applied over half the vehicle body and the wet tank solution applied over the other half.

The wing weight of wing-body concepts is estimated by an empirical formula given in reference 3. In terms of the wing parameters, this formula is

$$W_{wing} = 2.49\ (1.0) C_{MW} \left[\frac{W_{TO}{}^2\, n}{0.02\ (W/S) \tan\ \Lambda} \right]^{0.5375} \qquad \text{(B42)}$$

where n is the load factor and C_{MW} is a materials coefficient (0.0352 for the advanced concept) which increases with temperature. A wing thickness ratio of 0.04 was used in this study.

APPENDIX C

BUCKLING EQUATIONS

In this appendix expressions are derived for the equivalent isotropic thickness of the shell required to preclude buckling $\bar{t}_{S_B}$ and for the "smeared" equivalent isotropic thickness of the ring frames required to preclude general instability $\bar{t}_F$. The expressions are derived for the elliptical shell of the all-body configuration; these expressions are then used to obtain the equations for cylindrical shells as a special case.

For the sandwich shell concept, it is assumed that the elliptical shell buckles at the load determined by the maximum compressive stress resultant N_x^-, on the ellipse. Reference 33 indicates that a good approximation is obtained by assuming the structure to be a circular cylinder with the same radius of curvature as that of the ellipse at the point of application of N_x^-. Since the maximum load occurs at the ends of the minor axis where the radius of curvature is a^2/b, the buckling equation is

$$\frac{N_x^-}{(a^2/b)E} = \epsilon \left[\frac{\bar{t}_{S_B}}{(a^2/b)} \right]^m$$

or, solving for $\bar{t}_{S_B}$

$$\bar{t}_{S_B} = (a^2/b) \left[\frac{N_x^-}{(a^2/b)E\epsilon} \right]^{1/m} \tag{C1}$$

This equation is based on small deflection theory, which seems reasonable for sandwich cylindrical shells, although it is known to be inaccurate for monocoque cylinders. Values of m and ϵ may be found in reference 16 for both monocoque and truss-core sandwich. For the nominal potential concept, m is 1.667 and ϵ is 0.3615. For the wing-body, this expression becomes

$$\bar{t}_{S_B} = r \left(\frac{N_x^-}{rE\epsilon} \right)^{1/m} \tag{C1'}$$

The quantities N_x^-, a, b, r, and consequently $\bar{t}_{S_B}$, will vary with body station dimension x. As mentioned earlier, frames are not used with sandwich concepts.

For the stiffened shell concept, the common procedure of assuming the shell to be a wide column is adopted. The buckling equation is then (ref. 16)

$$\frac{N_x^-}{dE} = \epsilon \left(\frac{\bar{t}_{S_B}}{d} \right)^2$$

or, solving for $\bar{t}_{S_B}$

$$\bar{t}_{S_B} = \sqrt{\frac{N_x^- d}{E\epsilon}} \tag{C2}$$

which is applicable both for the all-body and the wing-body. For the nominal advanced concept, ϵ is 0.911. This concept requires frames to prevent general instability failures.

In order to generalize the Shanley criterion for frame sizing to elliptical shells, the stiffness of elliptical rings to inplane loads must be determined. If the methods and nomenclature of reference 32 (sec. 81) are used, the redundant bending moment at the ends of the semimajor axis of an elliptical ring due to opposing inplane point loads of magnitude L acting perpendicular to the ring at the ends of the semiminor axis is

$$M_a = -\frac{\int^s M'ds}{\int^s ds} - \frac{L}{2}a$$

$$= \frac{L}{2aE_{II}} \int_0^a \sqrt{\frac{a^4 - a^2y^2 + b^2y^2}{a^2(a^2 - y^2)}}\, dy - \frac{L}{2}a$$

$$= \frac{La}{4}\left(\frac{E_{III}}{E_{II}} - 2\right) \tag{C3}$$

where the dimensional quantities are defined in figure 24 and

$$E_{III} = 1 + \frac{\log_e [(a/b)(1 + e)]}{(a/b)^2 e} \tag{C4}$$

The bending-moment distribution in the ring, therefore, is given by

$$M = \frac{La}{4}\left(\frac{E_{III}}{E_{II}} - 2\frac{y}{a}\right) \tag{C5}$$

To determine the deflection of the ring at the point of application of the load, the method of virtual work is used:

$$\delta = 2\int^s \frac{M(M/L)}{EI_F}\, ds$$

$$= \frac{2L}{EI_F}\int_0^a \left(\frac{aE_{III}}{rE_{II}} - \frac{y}{2}\right)^2 \sqrt{1 + \frac{b^2y^2}{a^2(a^2 - y^2)}}\, dy$$

$$= \frac{La^3}{EI_F}\left(\frac{2E_{II} - E_I}{6} + \frac{E_I - E_{II}}{6e^2} - \frac{E_{III}^2}{8E_{II}}\right) \tag{C6}$$

Since $L = K_S\delta$, the spring constant of the ring is

$$K_S = \frac{K_3 EI_F \left(\frac{\pi}{8} - \frac{1}{\pi}\right)}{8a^3\left(\frac{2E_{II} - E_I}{6} + \frac{E_I - E_{II}}{6e^2} - \frac{E_{III}^2}{8E_{II}}\right)} \tag{C7}$$

the factor $(K_3/8)[(\pi/8) - (1/\pi)]$ being added to conform to reference 14.

It is of interest to compare the stiffness of an elliptical ring to that of a circular ring. For equal values of EI_F and equal enclosed areas ($r = \sqrt{ab}$), the ratio of spring constants is

$$\frac{(K_S)_{ellipse}}{(K_S)_{circle}} = \frac{2\left(\frac{b}{a}\right)^{3/2}\left(\frac{\pi}{8} - \frac{1}{\pi}\right)}{\frac{2E_{II} - E_I}{3} + \frac{E_I - E_{II}}{3e^2} - \frac{E_{III}^2}{4E_{II}}} \tag{C8}$$

This ratio is plotted as a function of a/b in figure 29, and the relatively low spring constant of the elliptical ring at the values of a/b of interest indicates that the weight of the rings in elliptical shells will be greater than those of circular shells for the same conditions.

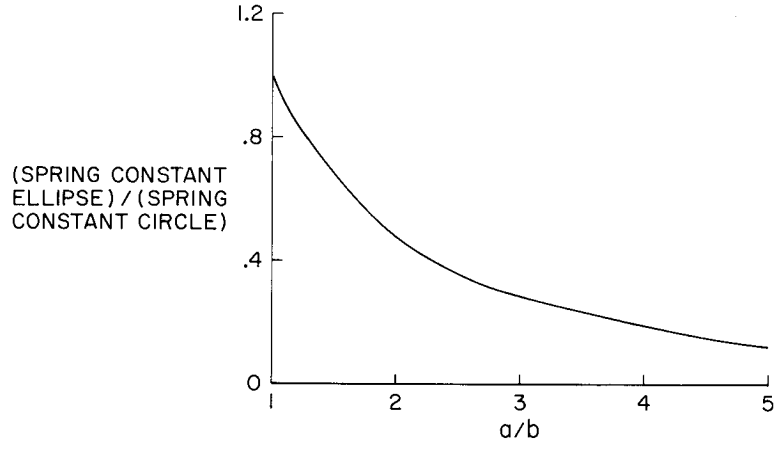

Figure 29.– Comparison of spring constants of elliptic and circular frames.

The equation for frame (ring) weight is next established. Generalizing the results of reference 14 to elliptical frames gives the following expression for the spring constant required of the frames

$$K_S = \frac{K_1 K_2 a E_{II} N_x^-}{d} \tag{C9}$$

If the frames are "smeared" according to $A_F = \bar{t}_{F_B} d$, then combination of equations (C7) and (C9) gives

$$\bar{t}_{F_B} = \sqrt{\frac{4C_F N_x a^4 E_{II}\left(\frac{2E_{II} - E_I}{3} + \frac{E_I - E_{II}}{3e^2} - \frac{E_{III}^2}{4E_{II}}\right)}{K_{F1} d^3 E\left(\frac{\pi}{8} - \frac{1}{\pi}\right)}} \tag{C10}$$

where K_{F1} is defined by equation (B8), and where the constants K_1, K_2, K_3 have been absorbed by "Shanley's constant," C_F, taken to be 0.625×10^{-4} in this study. Calculations show that the expression

$$\bar{t}_{F_B} = \sqrt{\pi C_F N_x / K_{F1} d^3 E}\ \sqrt{3 + (b/a)}(0.3719ab + 0.6281a^2) \tag{C11}$$

very closely approximates equation (C10) for the range of a/b of interest and equation (C11) is used in the weight analysis.

Since the frame spacing, d, is as yet unspecified, it may be chosen to minimize the shell plus frame weight. If the structure is buckling critical, the total equivalent thickness is

$$\bar{t} = \bar{t}_{S_B} + \bar{t}_{F_B} \tag{C12}$$

where $\bar{t}_{S_B}$ and $\bar{t}_{F_B}$ are given by equations (C2) and (C11). When $\bar{t}$ is minimized with respect to d,

$$\left.\begin{aligned} \bar{t} &= \frac{4}{27^{1/4}}\left(\frac{\pi C_F}{K_{F1}\epsilon^3}\right)^{1/8}\left(\frac{N_x}{E}\right)^{1/2}\left[\sqrt{\left(3 + \frac{b}{a}\right)}(0.3719ab + 0.6281a^2)\right]^{1/4} \\ \bar{t}_{S_B} &= \frac{3}{4}\bar{t} \\ \bar{t}_{F_B} &= \frac{1}{4}\bar{t} \end{aligned}\right\} \tag{C13}$$

where the optimum frame spacing is given by

$$d = \left[3\sqrt{\frac{\pi C_F \epsilon}{K_{F1}}}\sqrt{3 + \frac{b}{a}}\,(0.3719ab + 0.6281a^2)\right]^{1/2} \tag{C14}$$

Note that from equation (C13) the shell weight is three times the frame weight for optimum design. Reduction of equations (C13) and (C14) to the case of a circular section gives the equations for the wing-body

$$\left.\begin{aligned} \bar{t} &= \frac{4}{27^{1/4}} \left(\frac{\pi C_F}{K_{F1}\epsilon^3}\right)^{1/8} \left(\frac{N_x}{E}\right)^{1/2} (2r^2)^{1/4} \\ \bar{t}_{S_B} &= \frac{3}{4}\,\bar{t} \\ \bar{t}_{F_B} &= \frac{1}{4}\,\bar{t} \end{aligned}\right\} \qquad \text{(C13')}$$

$$d = \left(6r^2 \sqrt{\frac{\pi C_F \epsilon}{K_{F1}}}\right)^{1/2} \qquad \text{(C14')}$$

It is of interest to note that equation (C13) is in the form

$$\bar{t} \sim \begin{pmatrix}\text{structure}\\ \text{coefficient}\end{pmatrix}^{1/8} \begin{pmatrix}\text{load-material}\\ \text{coefficient}\end{pmatrix}^{1/2} \begin{pmatrix}\text{geometry}\\ \text{coefficient}\end{pmatrix}^{1/4} \qquad \text{(C15)}$$

Hence, the parameters which describe the structure, and which are most likely the least well defined, enter into this equation in only the 1/8 power.

REFERENCES

1. Roland, H. L.: Advanced Design Weight Analysis and Systems and Equipment Weight Prediction. 28th Annual Conference on Mass Properties Engineering, SAWE, Paper no. 790, San Francisco, May 5–8, 1969.

2. General Dynamics/Astronautics: Weight Estimation of Hypersonic Airbreathing Aircraft. NASA Contract NAS 2–1870, October 1964, Final Reports GD/A–DCB–64–073 I, II, and 089A.

3. General Dynamics/Convair: Weight and Size Analyses of Advanced Cruise and Launch Vehicles. NASA Contract NAS 2–3025, March 1966, Final Reports GD/C–DCB–66–008/1–8.

4. Weber, R. J.: Propulsion for Hypersonic Transport Aircraft. Fourth Congress International Council Aerospace Sciences, Paris, Aug. 24–28, 1964. Paper 64–558.

5. Knip, G. Jr.; and Allen, J. A.: Analysis of Booster Systems With a Recoverable Hypersonic Airplane First Stage. AIAA Paper 64–543.

6. Gregory, T. J.; Petersen, R. H.; and Wyss, J. A.: Performance Tradeoffs and Research Problems for Hypersonic Transports. AIAA Paper 64–605, J. Aircraft, vol. 2, no. 4, July–Aug. 1965, pp. 266–271.

7. Jarlett, F. E.: The Hydrogen Fueled Hypersonic Transport. Proc. 1968 Annual Aviation and Space Conference, ASME, Beverly Hills, Ca., June 16–19, 1968, pp. 464–470.

8. Petersen, R. H.; Gregory, T. J.; and Smith, C. L.: Some Comparisons of Turboramjet-Powered Hypersonic Aircraft for Cruise and Boost Missions. AIAA Paper 65–759, J. Aircraft, vol. 3, no. 5, Sept.–Oct. 1966, pp. 398–405.

9. Jarlett, F. E.: Performance Potential of Hydrogen Fueled, Airbreathing Cruise Aircraft. General Dynamics/Convair Division, Report no. GD/C–DCB–66–004/1, 1966.

10. Gregory, T. J.; Ardema, M. D.; and Waters, M. H.: Hypersonic Transport Preliminary Performance Estimates for an All-Body Configuration. AIAA Paper 70–1224, 1970.

11. Gregory, Thomas J.; Williams, Louis J.; and Wilcox, Darrell E.: The Airbreathing Launch Vehicle for Earth Orbit Shuttle-Performance and Operation. AIAA Paper 70–270, 1970.

12. Heldenfels, Richard R.: Structural Prospects of Hypersonic Air Vehicles. ICAS Paper 66–31, 5th Congress of the International Council of the Aeronautical Sciences, London, England, September 12–16, 1966.

13. Ardema, Mark D.: Analysis of Bending Loads of Hypersonic Aircraft. NASA TM X–2092, 1970.

14. Shanley, Francis R.: Weight-Strength Analysis of Aircraft Structures. Second ed., Dover, New York, 1960.

15. U.S. Dept. of Defense: Metallic Materials and Elements for Aerospace Vehicle Structures. MIL–HDBK–5A, 1966.

16. Crawford, R. F.; and Burns, A. B.: Minimum Weight Potentials for Stiffened Plates and Shells. AIAA J. vol. 1, no. 4, April 1963, pp. 879–886.

17. Rivello, Robert M.: Theory and Analysis of Flight Structures. McGraw–Hill, 1969.

18. Timoshenko, Stephen P.; and Gere, J. M.: Theory of Elastic Stability. Second ed., McGraw–Hill, 1961.

19. Sterett, James B., Jr.: Shell Stability Problems in the Design of Large Space Vehicle Boosters. NASA TN D–1510, 1962.

20. General Electric Company: Study of Structural Weight Sensitivities for Large Rocket Systems. NASA CR–73087, 1967.

21. Anon.: Buckling of Thin-Walled Circular Cylinders. NASA SP–8007.

22. Block, David L.: Influence of Ring Stiffeners on Instability of Orthotropic Cylinders in Axial Compression. NASA TN D–2842, 1964.

23. Hedgepeth, John M.; and Hall, D. B.: Stability of Stiffened Cylinders. AIAA J., vol. 3, no. 12, Dec. 1965, pp. 2275–2286.

24. Boley, Bruno A.; and Weiner, Jerome H.: Theory of Thermal Stresses. John Wiley, 1960.

25. Plank, P. P.; Sakata, I. F.; Davis, G. W.; and Richie, C. C.: Hypersonic Cruise Vehicle Wing Structure Evaluation. NASA CR–1568, 1970.

26. Heathman, John H.; et al.: Hydrogen Tankage Application to Manned Aerospace Systems. Phases II & III, vol. I, AFFDL–TR–68–75, 1968.

27. Ardema, Mark D.: Solutions of Two Heat-Transfer Problems With Application to Hypersonic Cruise Aircraft. NASA TM X–2025, 1970.

28. Jackson, L. Robert; Davis, John G., Jr.; and Wichorek, Gregory R.: Structural Concepts for Hydrogen-Fueled Hypersonic Airplanes. NASA TN D–3162, 1966.

29. Becker, J. V.: New Approaches to Hypersonic Aircraft. 7th Congress of the International Council of the Aeronautical Sciences. ICAS Paper 70–16.

30. Williams, Louis J.: Estimated Aerodynamics of All-Body Hypersonic Aircraft Configurations. NASA TM X–2091, 1971.

31. Waters, Mark H.: Turbojet-Ramjet Propulsion System for All-Body Hypersonic Aircraft. NASA TN D–5993, 1971.

32. Timoshenko, Stephen P.; and Young, D. H.: Theory of Structures. McGraw–Hill, 1945.

33. Hutchinson, J. W.: Buckling and Initial Postbuckling Behavior of Oval Cylindrical Shells Under Axial Compression. ASME Paper 67–APM–W, Dec. 1966.

NASA-Langley, 1972 —— 32 A–3905